Review

Carbon Future

Metal oxide semiconductor-based methane sensing

Renjie Chen[1], Shuyu Lin[1], Zhongtian Wang[2], Yi Xia[3]✉, and Lan Xiang[1]✉

[1] *Department of Chemical Engineering, Tsinghua University, Beijing 100084, China*
[2] *Tanwei College, Tsinghua University, Beijing 100084, China*
[3] *Research Center for Analysis and Measurement, Kunming University of Science and Technology, and Analytic & Testing Research Center of Yunnan, Kunming 650093, China*

Cite This: *Carbon Future* **2025**, *2*, 9200037

Read Online

ABSTRACT: Real-time and sensitive detection of methane (CH_4) is vital to the safety of life and production due to the explosivity and greenhouse effect of methane. Currently, metal oxide semiconductor (MOS)-based chemiresistive sensors are considered as an effective approach for their low cost, highly tunable structures, and easy fabrication. However, disadvantages like high working temperature, low sensitivity, and unsatisfying selectivity limit their potential wide application. In order to achieve the goal of high-performance MOS-based methane sensors, in this review, from the basic mechanism of MOS-based gas sensing and the property of methane, possible strategies of improving methane sensing performances in multiple aspects have been summarized systematically, including sensitivity, selectivity, stability, and humidity resistance. Recent progress in the research and development of metal oxide semiconductor-based methane sensor technology is also surveyed in this review. Finally, the future trends and perspectives of MOS-based chemiresistive methane sensors are proposed.

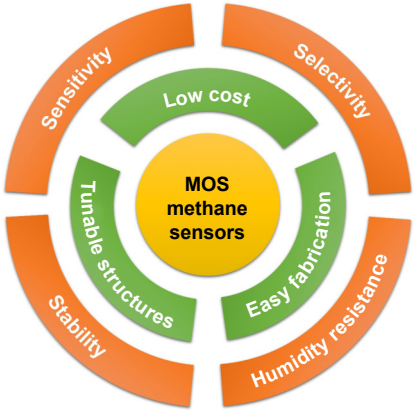

KEYWORDS: CH_4 sensors, metal oxide semiconductors, sensitivity, selectivity, stability, humidity resistance

1 Introduction

Methane (CH_4) is the simplest alkane with the highest C/H ratio and widely used as fuel owing to its high calorific value. It is also an important raw material for many chemicals, such as ethylene, hydrogen, and chloromethane[1]. In recent years the extraction of CH_4-bearing resources such as shale gas[2], natural gas[3], coalbed CH_4[4], and CH_4 hydrate resources[5] is continuously growing. However, CH_4 is also an explosive gas with an explosion range of 4.9%–15.4%[6], and a greenhouse gas equivalent of more than 25 times of CO_2[7]. With the aim of utilizing CH_4 resources safely as well as monitoring the greenhouse effect, it's essential to develop advanced CH_4 sensors to detect the concentration of CH_4 accurately and quickly.

CH_4 consists of four identical C–H bonds with a tetrahedral symmetric structure formed by sp^3 hybridization, where each C–H bond energy is as high as 414 kJ·mol^{-1}, and there is neither π bond nor non-bonded electron pair in CH_4[9]. From the viewpoints of molecular orbital theory, there are two ways to weaken the C–H bond in CH_4: to seize one electron from the bonding orbital or to inject one electron into the antibonding orbital. It is quite difficult to weaken the C–H bond in CH_4 due to the low energy of the highest occupied molecular orbit (HOMO) and the high energy of the lowest unoccupied molecular orbit (LUMO)[10], as shown in **Fig. 1**. The low intrinsic reactivity of CH_4 still inhibits the development of CH_4 sensing.

Up to now, many techniques have been developed to sensing CH_4, including catalytic combustion[11], spectroscopy[12], electrochemistry[13], acoustics[14], etc. Present commercial CH_4 sensors mainly consist of the infrared spectroscopy sensors and catalytic combustion sensors, and the latter is in majority[15]. The infrared spectroscopy sensor relies on the spectral absorption of CH_4 to the light of specific wavelength, and has the advantages of low limit of detection (2 ppb), high selectivity, and fast response (< 30 s)[16]. However, the high fabrication cost of the optical components hinders their wide application. The catalytic combustion sensor realizes CH_4 sensing by detecting the resistance change of sensitive components caused by catalytic combustion heat of CH_4. Despite the low cost and fast response (< 30 s), catalytic combustion sensor is prone to deactivate due to poisoning such as coking. Therefore, manual calibration is required every 7–10 days in practical[17]. In the interest of developing next generation CH_4 sensors, metal oxide semiconductors (MOS) have attracted much attention owing to their low cost, flexibility, highly tunable structures, and easy fabrication[18, 19]. MOS CH_4 sensors undergo resistance change upon

Received: December 12, 2024; **Revised:** January 15, 2025
Accepted: January 18, 2025

✉Address correspondence to Yi Xia, xiayi0125@163.com; Lan Xiang, xianglan@mail.tsinghua.edu.cn

https://doi.org/10.26599/CF.2025.9200037

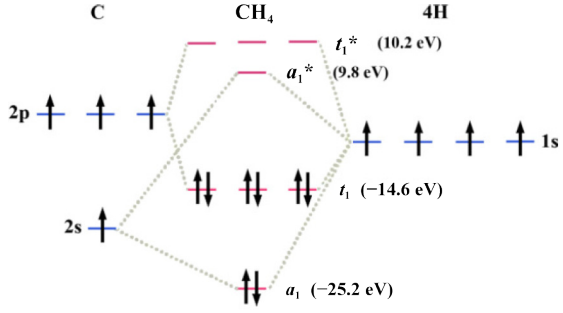

Fig. 1. Molecular orbital diagrams of CH_4. Reproduced with permission from Ref.[8], © Shah et al. 2020.

exposure to CH_4 by electron transferring reaction between CH_4 and surface chemisorbed oxygen, and n-type MOS whose majority carrier is electron undergoes resistance increase while p-type MOS whose majority carrier is hole undergoes resistance decrease. In general, n-type MOS is more used in CH_4 sensing since their conduction band electron mobility (SnO_2: 160 $cm^2 \cdot V^{-1} \cdot s^{-1}$; ZnO: 200 $cm^2 \cdot V^{-1} \cdot s^{-1}$; and In_2O_3: 15–100 $cm^2 \cdot V^{-1} \cdot s^{-1}$) is higher than that of the positive holes of p-type MOS (NiO: 0.2 $cm^2 \cdot V^{-1} \cdot s^{-1}$)[20], which favors the CH_4 sensing. In recent 10 years, MOS-based material accounts for more than 50% in CH_4 sensing material studies[21], and it is the most potential candidate for next-generation CH_4 sensor.

A brief CH_4 sensing mechanism should be introduced for better understanding the challenges in CH_4 sensing. Oxygen adsorption model and electron depletion layer are widely accepted in present CH_4 sensing mechanism. Here n-type MOS was selected as an example for mechanism demonstration. When MOS sensors are exposed to atmosphere, the electron would transfer from conduction band of MOS to oxygen molecules adsorbed on the surface because the electron affinity of oxygen is higher than the work function of metal oxides, causing the band bending on the surface of MOS. Then the adsorbed oxygen transforms to different ionized species (< 150 °C: O_2^-, and 150–400 °C: O^-)[22]. The layer of charged oxygen creates a region depleted of electrons on the surface. As illustrated in **Fig. 2**, a core–shell structure formed with depletion layer as shell.

When CH_4 is introduced, chemisorbed oxygen plays the main role in CH_4 sensing by CH_4 oxidation[23]

$$CH_4\,(ad) + 2O_2^-\,(ad) \rightarrow CO_2\,(ad) + 2H_2O + 2e^- \quad (1)$$

$$CH_4\,(ad) + 4O^-\,(ad) \rightarrow CO_2\,(ad) + 2H_2O + 4e^- \quad (2)$$

The overall resistance R_{total} of the MOS-based sensor is determined by the resistance of both core and shell (denoted as R_{core} and R_{shell}, respectively). For n-type MOS sensors, $R_{shell} >> R_{core}$ because electrons are depleted in the shell. Thus, R_{total} is dominated by R_{shell}. In CH_4 sensing, the generated electrons are reinjected in the conduction band of MOS, and the band bending is therefore decreased with the narrowed depletion layer. Thus, R_{shell} is decreased and sensing signal is generated by measuring the resistance of the MOS sensor[24].

However, MOS CH_4 sensors still suffer from problems such as the insufficient sensitivity, low selectivity, and poor long-term stability, as illustrated in **Fig. 3**. Compared with recent reviews on MOS-based CH_4 sensing[23, 25, 26], here in this review, we mainly focus on the problems in recent MOS CH_4 sensing studies in the aspects of sensitivity, selectivity, stability, and humidity resistance from the perspective of sensitive materials, and pay less attention on the sensor fabrication, data processing, or the hazard of CH_4 emission. Moreover, we have also summarized the corresponding possible solutions on the level of materials, including recently explored breakthroughs. Finally, based on the discussions, the future outlooks of MOS-based CH_4 sensors have been put forward.

2 Challenges and approaches in MOS CH_4 sensing

There are seven aspects to evaluate the performance of gas sensors: (1) sensitivity, (2) selectivity, (3) response/recovery time, (4) energy consumption, (5) reversibility, (6) adsorptive capacity, and (7) fabrication cost. All these factors are essential for a successful gas sensor. For MOS-based CH_4 sensors, we chose some of the most concerned factors to discuss in detail.

2.1 Response/sensitivity/response and recovery time

Response and response/recovery time are the main factors to evaluate the sensitivity of MOS CH_4 sensors. Response is usually

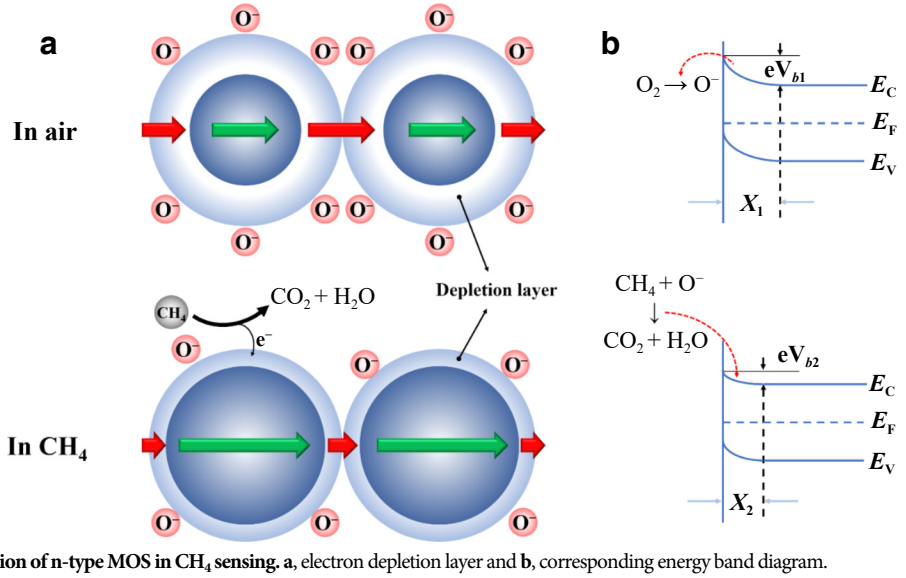

Fig. 2. Schematic illustration of n-type MOS in CH_4 sensing. a, electron depletion layer and **b**, corresponding energy band diagram.

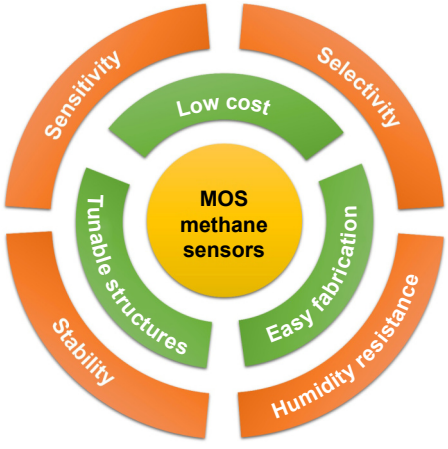

Fig. 3. Advantages and existing problems of MOS-based CH_4 sensors.

defined as $R = (R_a - R_g)/R_g \times 100\%$ for n-type MOS, or $R = (R_g - R_a)/R_a \times 100\%$ for p-type MOS in CH_4 sensing, where R_a and R_g are the resistance of MOS in air and in CH_4, respectively. In actual CH_4 sensing, R_a is not a constant and is always fluctuating due to the dynamic atmosphere. A high response can effectively reduce the influence of R_a fluctuation, thereby improving the sensing accuracy. Compared with other gases, response of MOS CH_4 sensors is relativity low. In a case using ZnO nanorods as sensing materials, the response to 40 ppm NO_2 is 30 times that to 40 ppm CH_4 at 300 °C[27]. The low response to CH_4 results from its intrinsic low reactivity. The stable response to CH_4 comes from the chemical equilibrium CH_4 oxidation reaction and oxygen adsorption reaction. The low CH_4 oxidation rate led to a small change of the amount of chemisorbed oxygen, which determines the resistance of MOS. Thus, the response to CH_4 is usually relatively small compared to other gases.

Response/recovery time is defined as the time required for 90% variation of the resistance in the response/recovery progress. Real-time sensing of CH_4 is critical considering its explosiveness, which requires short response/recovery time. According to Chinese standards on combustible gas detectors for household and industry, the response time should be less than 30 s[28]. Factors that influence response/recovery time can be ascribed in two aspects. The first is the adsorption and desorption kinetics. In the response process, a high adsorption rate of both CH_4 and oxygen would shorten the time required to reach the aforementioned chemical equilibrium. In the recovery process, it is proposed that the time-limiting process is chemisorption of oxygen. Thus, acceleration of oxygen adsorption would also shorten the recovery time[29, 30]. A facile way to shorten response/recovery time is to increase working temperature to accelerate the adsorption/desorption process. At high temperature around 300 °C, the typical response time of CH_4 MOS sensor is less than 1 min[31–33]. In recent years, low working temperature (< 150 °C) and even room temperature MOS CH_4 sensors have been developed. The low adsorption/desorption rate at low temperature led to the prolonged response/recovery time, usually more than 5 min[34–36]. The second factor is the charge carrier mobility. With a higher mobility, the local conductivity change can be quickly spread to the whole material. Thus, the response/recovery time is also shortened. For example, increasing electron mobility can be realized by reducing the electron scattering caused bulk defects, and ZnO nanorods with less bulk defects showed a response/recovery time of 60 s/5 s in ozone detecting at room temperature, compared with the response/recovery time of 220 s/35 s of ZnO nanorods with more bulk defects.[37]

2.1.1 *Structure modification*

As the sensing process is based on the catalytic oxidation of CH_4, some general methods in catalysis enhancement could also be applied in sensitivity improvement. One of them is porous structure and larger specific surface area. Zhou et al. synthesized zinc oxide nanobulk, nanofibers, and nanorods with the same hydrothermal route but different surfactant additions. The specific surface areas of nanobulk, nanofibers, and nanorods are 19.7, 26.4, and 28.6 $m^2 \cdot g^{-1}$, and the average surface pore sizes are 10, 16, and 18 nm, respectively. Their response values to 200 ppm methane at 270 °C are 62.38%, 88.27%, and 100.49%, respectively, with the ZnO nanofibers showing the greatest sensitivity (**Fig. 4a**)[38]. Gas sensing reactions occur on the surface of sensitive materials, and the diffusion of gas molecules in the material and the adsorption on the material surface are the basis of sensing. The microstructure of sensitive materials directly affects their adsorption performance for gases. A high specific surface area is beneficial for increasing the adsorption reaction active sites on the surface of sensitive materials, while a porous structure is conducive to the diffusion and adsorption of gases in sensitive materials[39].

The grain size also has a great influence on the sensing behavior of MOS. As described above, the total resistance of MOS R_{total} is dominated by R_{shell}, because electrons are depleted in the shell. And for the semiconductor, the length of the electron depletion layer, also called as Debye layer λ_d, is determined by Eq. (3)[40]

$$\lambda_d = \left(\frac{\varepsilon kT}{q^2 n_c}\right)^{\frac{1}{2}} \tag{3}$$

where ε, k, T, q, and n_c represent the dielectric constant, the Boltzmann constant, the temperature, the charge of electron, and the carrier concentration, respectively. It could be derived that for a certain type of semiconductor at a certain temperature, its Debye length is fixed. Therefore, if the grain size of a semiconductor is less than twice the width of its Debye length, then the core is eliminated, and the electrons in all parts of the material could be affected by sensing reactions, enhancing the sensing performance, as shown in Fig. 4b[22]. Alenezi et al. prepared ZnO nanosheets with a diameter of ~ 30 μm and thicknesses of 150, 100, and 50 nm, respectively. It is found that the smaller the thickness of ZnO nanosheets, the better its response to ethanol. At 300 °C, ZnO nanosheets with the thicknesses of 150, 100, and 50 nm showed a response of 28, 45, and 403 to 500 ppm ethanol, respectively. When the thickness approached twice the Debye length of ZnO (46 nm), the gas sensing performance was significantly improved[41].

In recent years, researchers have found that defects in semiconductor oxides can affect the gas sensing performance of materials, with surface oxygen vacancy (OV) defects being the most common. The presence of surface defects such as oxygen vacancies not only affects the concentration of charge carriers in semiconductor oxides, but also has an impact on their gas adsorption performance[42, 43]. Hussain et al. calculated the effect of oxygen vacancies on the methane sensing performance of ZnO with density functional theory (DFT), and proposed that an increase in oxygen vacancy concentration is beneficial for improving the methane sensing performance of ZnO[44]. Firstly, the surface energy at the oxygen vacancy site is high, which is conducive to gas adsorption. Secondly, the oxygen vacancy

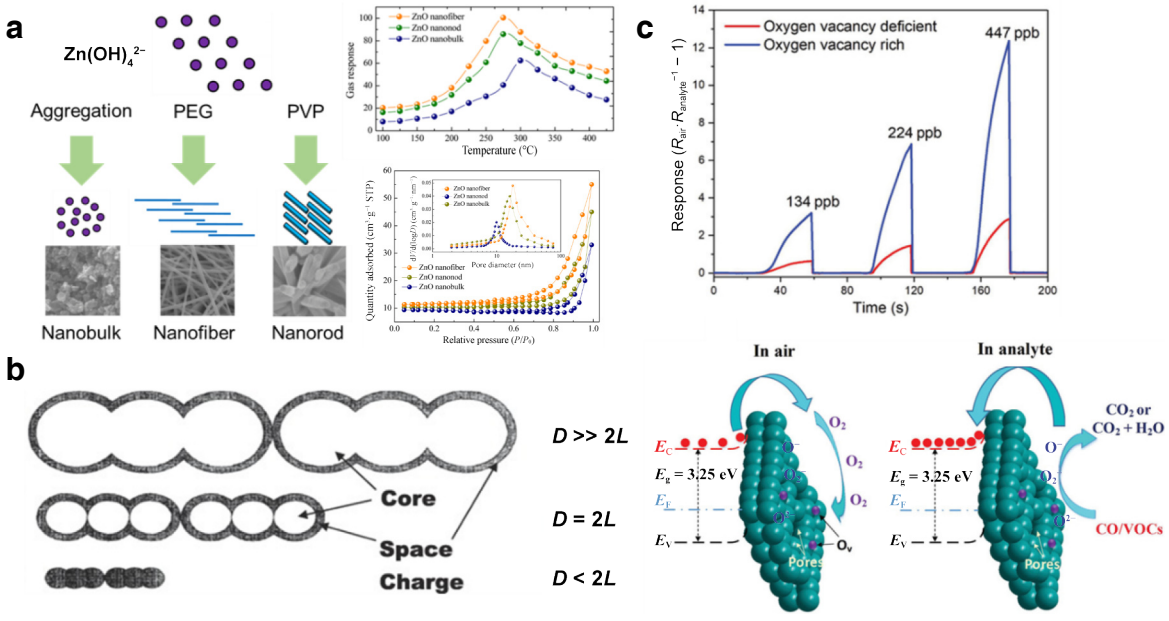

Fig. 4. Strategies for improving CH_4 sensitivity via structure modification. a, The influence of morphology and specific surface area of ZnO on CH_4 sensitivity. Reproduced with permission from Ref.[38], © Zhou, Q. et al. 2013. **b**, Mechanisms of grain size dependence of conductance in semiconductor gas sensing materials. Reproduced with permission from Ref.[22], © Elsevier B.V. 2018. **c**, Dynamic response of sensors with variant amounts of oxygen vacancies to different CO concentrations at 300 °C, and schematic diagram of gas sensing mechanism of oxygen vacancy-rich ZnO nanosheets. Purple spheres stand for oxygen vacancies. Reproduced with permission from Ref.[45], © WILEY-VCH Verlag GmbH & Co. KGaA, Weinheim 2019.

increases the free electron concentration of ZnO, which is conducive to the formation of surface adsorbed oxygen.

Yuan et al. synthesized hierarchical ZnO with different surface oxygen vacancy contents via a two-step method. They first synthesized the metal organic framework (MOF) material ZIF-L (ZIF = zeolitic imidazolate framework), and then decomposed ZIF-L into ZnO under high temperature. By controlling the heating rate in the high-temperature decomposition step, ZnO with different surface oxygen vacancy contents can be obtained. The ZnO prepared by this method can respond to CO of ppb level at 300 °C, and the ZnO rich in surface oxygen vacancies (prepared at a heating rate of 10 °C·min^{-1}) has a much higher response value to 447 ppb CO (24.9) than the ZnO with less surface oxygen vacancies (14.5), which was prepared at a heating rate of 2 °C·min^{-1} (Fig. 4c)[45]. Ahn et al. prepared ZnO nanorods with different surface oxygen vacancy contents and investigated their NO_2 sensing performance. The results showed that the response performance of ZnO nanorods to NO_2 was positively correlated with the surface oxygen vacancy content of ZnO, and proposed that the enhanced adsorption of NO_2 on ZnO surface by oxygen vacancies was one of the reasons for the improved response performance[46].

2.1.2 *Electronic sensitization*

When two dissimilar materials build a heterojunction, the electrons at higher energy state will flow across the interface to unoccupied lower energy state until the whole Fermi level reaches equilibrium, which is referred as electronic sensitization[47]. There are two main types of heterojunctions: semiconductor–semiconductor and metal–semiconductor, and the former consists of p–n, n–n, and p–p heterojunction[48]. A schematic explanation of charge transfer of p–n and n–n type heterojunction is presented in **Fig. 5**. For p–n junction, the electron–hole recombination at the interface would increase the overall resistance since the free charge carrier is depleted. The increased initial resistance favors the n-type MOS CH_4 sensing more than p-type MOS because the resistance decline (n-type CH_4 sensing) was more dramatical when initial resistance was higher[48]. As demonstrated in Zhang's work[31, 49], p-NiO decorated n-ZnO (32.9 MΩ) and n-SnO_2 decorated p-NiO (2.2 kΩ) both showed higher initial resistance than pure ZnO (5.12 MΩ) and NiO (0.93 kΩ), respectively. ZnO/NiO showed four times higher response (54.5%) than pure ZnO (13.5%) to 6000 ppm CH_4, while NiO/SnO_2 showed three times higher response (48.9%) than pure NiO (15.4%) to 7000 ppm CH_4. For n–n junction, since charge carriers in both sides are electrons, the electron transfer is determined by energy level. As demonstrated in Figs. 5c and 5d, the electrons of TiO_2 migrate to SnO_2 due to higher conduction band edge energy (E_{CB}) of TiO_2 than SnO_2. Compared with the depletion layer at the interface of p–n junction, n–n junction forms an "accumulation layer" on SnO_2 side and "depletion layer" on TiO_2 side. The electron accumulation facilitates additional oxygen adsorption on SnO_2 side[48]. Li et al. synthesized the graphite carbon nitride (g-C_3N_4) modified ZnO (ZnO/g-C_3N_4), which showed two times higher response (11.9) to 1000 ppm CH_4 at 320 °C than pure ZnO (5.3). Because the Fermi level of g-C_3N_4 is higher than ZnO, the electrons of g-C_3N_4 would migrate to ZnO, which facilitates the formation of chemisorbed oxygen. Besides, on contacting of CH_4, g-C_3N_4 and ZnO both acted as CH_4 reaction sites and the additional electrons trapped on g-C_3N_4 because CH_4 oxidation would migrate to ZnO as well, which further reduced the resistance of ZnO and endowed a higher response[50]. Noble carbon materials like carbon nanotubes (single wall[51] or multiwall[52]) and graphene[53], as well as noble two-dimensional (2D) materials like g-C_3N_4, MXene[54], and transition metal dichalcogenides[55], have all been widely applied to form a heterojunction between the MOS to realize the electronic sensitization of CH_4 sensing.

It should be mentioned that the Schottky barrier at n–n junction can also increase the initial resistance when both semiconductors act as conduction path. In the work of Mondal et al., ZnO and

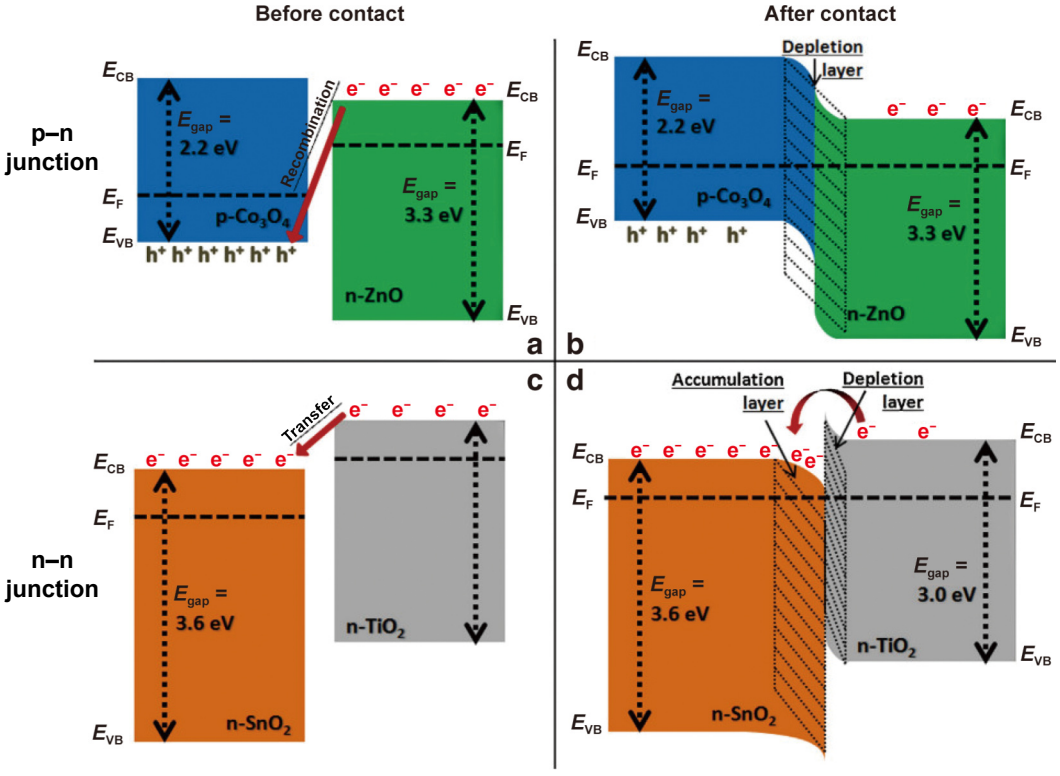

Fig. 5. Schematics explaining band bending at different heterojunction interfaces. **a**, p–n junction about to form between p-type Co_3O_4 and n-type ZnO. The available lower-energy valence band states (holes) stimulate electron transfer across the interface and the equilibrium of Fermi energies (E_F). **b**, Depletion layer formed on both sides of p–n junction due to recombination, creating a potential barrier for electron flow. **c**, n–n junction about to form between n-type SnO_2 and n-type TiO_2. The available lower-energy conduction band states stimulate electron transfer to n-SnO_2. **d**, Depletion layer formed at n-TiO_2 surface due to loss of electrons, and accumulation layer formed at SnO_2 surface due to added electrons. A potential barrier was also formed at the interface. E_{VB}: valence band edge energy, and E_{gap}: band gap energy. Reproduced with permission from Ref.[48], © Elsevier B.V. 2014.

SnO_2 both participated in construction of conducting channel, and the sensor showed higher initial resistance and response (300 kΩ, 31.5%) than pure ZnO (200 kΩ, 24%) to 0.5% CH_4[56].

Electronic sensitization can also be realized by metal–semiconductor heterojunction. Noble metals are usually used to construct such heterojunction considering their additional catalytic effect. The work function of n-type semiconductors Φ_s is smaller than that of metal in their electrically neutral states[57]. Thus, the intimate contacting of metal nanoparticles and metal oxides forms a Schottky barrier, with electron transferring from valence band of metal oxides to metal, and consequently the number of free electrons in the bulk is reduced. Besides, these accumulated oxygen atoms then capture electrons to form chemisorbed oxygen anions (O_2^-, O^-, and O^{2-}) as mentioned before and spillover to the surface of MOS[58]. Due to the formation of Schottky barrier and chemisorbed oxygen anions layer brought by the metal, the widths of local depletion layer around metal nanoparticles are widened, and thereby increasing the initial bulk resistance to endow an improved CH_4 sensing performance[59–61].

In addition to the heterojunction, electron sensitization can also be realized by light illumination. The light illumination is usually introduced to lower the operation temperature due to their low heat energy cost. At the illumination with energy exceeding the band gap of MOS, the electrons would be excited from the valence band to conduction band and activate the surface of MOS[62]. ZnO is usually applied in photocatalytic CH_4 conversion due to its high polar facet[63], which induces the formation of internal electrical field and promotes the activation of C–H bond[64]. With a band gap of 3.37 eV, ZnO can generate electrons under the light of wavelength less than 380 nm. The photogenerated electrons can migrate to the surface and lead to the formation of O^-, which is more active than O_2^-[65, 66]. From this point, researchers have achieved room temperature sensing based on ZnO under visible (VIS) or ultraviolet (UV)-light illumination to NO_2[67], ethanol[68], HCHO[69], etc. Still, there were few examples on CH_4. By using ZnO nanorods vertically grown on Si substrate, Kimiagar et al. reported a decreased optimal operating temperature from 225 to 100 °C under UV excitation compared with that in the dark, and the response to 1000 ppm CH_4 reached 68%, higher than that in the dark (~ 55%) at 225 °C[70]. However, the electron–hole recombination is a main factor that limited the efficiency of the light-assisted reactions[71], since the survival time of photogenerated electrons is too short to migrate to the surface and participate in redox reactions.

The construction of heterojunction also provides a solution to facilitate the separation of electrons and holes. For instance, by decorating g-C_3N_4 on ZnO, the photogenerated electrons would migrate to ZnO while photogenerated holes migrated to g-C_3N_4 since both the conduction band and valence band of ZnO were lower than those of g-C_3N_4. Thus, the g-C_3N_4 decorated ZnO showed room-temperature CH_4 sensing with higher response of 6.891 to 1000 ppm CH_4, 1.5 times more than that of pure ZnO (**Fig. 6a**)[72].

By decorating noble metal nanoparticles on MOS, the light required for electronic sensitization is extended to visible light region, which is safer and more energy-saving than UV light. The additional visible light adsorption results from the surface plasmon

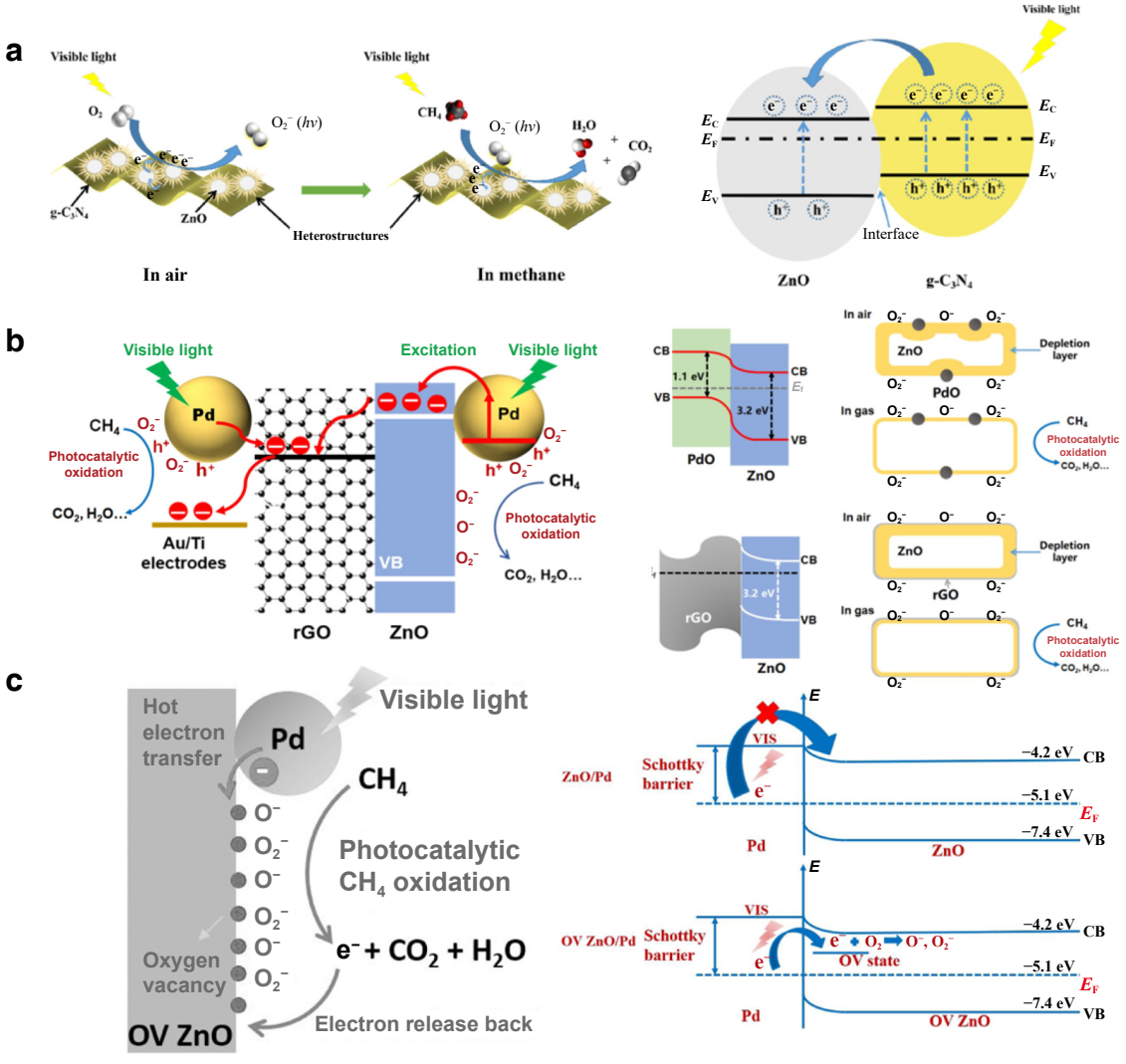

Fig. 6. Strategies for improving CH_4 sensitivity via electronic sensitization. a, The gas-sensing schematic diagram and energy band structure diagram of ZnO/g-C_3N_4 exposed to air and CH_4. Reproduced with permission from Ref.[72], © Elsevier Ltd. 2023. **b**, Schematic illustration of the mechanism for photocatalytic oxidation of CH_4, the improved electron transfer, and the multiple heterojunctions formed in the ternary rGO/ZnO/Pd hybrid under visible-light illumination. Reproduced with permission from Ref.[76], © Elsevier B.V. 2019. **c**, Schematic illustration of the mechanism of the photocatalysis-enhanced CH_4 sensing performance over the OV ZnO/Pd hybrid and the generation and transfer of hot electrons between Pd and ZnO. Reproduced with permission from Ref.[77], © Elsevier B.V. 2019.

resonance (SPR) of the metal when the frequency of incident light coincides with the oscillation frequency of free electrons on the metal surface[73]. Chen et al. reported the room-temperature CH_4 oxidation by Ag-decorated ZnO under visible light with a wavelength of 470 nm. The addition of Ag endowed a broadened absorption spectrum of ZnO in the visible light region (peaking at ~ 470 nm and extending to over 800 nm). The activated plasmonic Ag transferred the energetic electrons to MOS and sensitized the surface to enhance CH_4 oxidation[74]. Pd, as a superior CH_4 oxidation catalyst, was also reported to exhibit SPR peaks in the visible region[75]. We achieved room-temperature CH_4 sensing by Pd-decorated ZnO/rGO hybrid illuminated under visible light with a wave length of 470 nm. The sensor showed a response of 63.4% to 1% CH_4 and response/recovery time of 74 s/78 s. The photoexcited Pd transferred the excited electrons to ZnO and led to the formation of active oxygen species (O_2^- and O^-). Besides, Pd also promoted the dissociation of CH_4 and oxygen, which facilitates the catalytic oxidation of CH_4. Thus, both factors led to the exceptional room-temperature CH_4 sensing, as shown in Fig. 6b[76]. Then we further employed 590 nm visible light to realize CH_4 sensing at 80 °C by construction of Pd-decorated oxygen vacancy-enriched ZnO with a response of 36.8% to 0.1% CH_4. The Schottky barrier at the interface between Pd and ZnO hindered the transferring of excited electrons from Pd to ZnO. The introduction of surface oxygen vacancy-related energy level lowered the barrier for electron transferring, thus the electrons excited by 590 nm visible light can be transferred to oxygen vacancy to generate active O_2^- and O^- and improve CH_4 sensing performance (Fig. 6c)[77].

2.1.3 *Chemical sensitization*

Chemical sensitization is to accelerate CH_4 oxidation to improve the sensitivity. It is widely known that the low intrinsic reactivity is due to the difficulty of the C–H bond activation[78], so the general strategies of C–H activation could also be applied for better CH_4 sensing performance.

Usually, chemical sensitization is realized via noble metals loading owing to their catalytic ability on CH_4 oxidation. Pd is mostly employed in MOS CH_4 sensors due to its highest catalytic

activity towards methane oxidation[79–81]. Haridas et al. loaded multiple kinds of noble metal as well as metal-oxide catalysts (Pt, Ag, Ni, Pd, Au, NiO, and Au_2O_3) clusters onto SnO_2 thin film to find that Pd loaded SnO_2 exhibited the best sensing response for 200 ppm CH_4 in the temperature range of 80–220 °C, with the highest response of 97.2% at 220 °C[82]. The same improvement was also observed in Pd loaded ZnO-based sensor, where the response to 5000 ppm CH_4 increased from 9.0 to 19.2[83]. Nevertheless, in addition to Pd, other noble metals have also been applied in MOS CH_4 sensors, such as Pt[84], Au[85], and Ag[86], all of which showed enhanced CH_4 sensing performance.

It has been revealed that PdO (101) plays an important role in C–H bond cleavage from both experimental evidence and fundamental studies[87]. Pd (100) tends to be oxidized to PdO (101) in the presence of oxygen at elevated temperature[88]. The terminated PdO (101) surface consist of alternating rows of threefold or fourfold coordinated Pd or O, as shown in **Fig. 7**. The threefold coordinated Pd atoms are coordinatively unsaturated and constitute half of the surface Pd atoms. CH_4, with two C–H bonds as electron donor, coordinated with cu-Pd to form a σ-complex. The σ-complex formation weakens the coordinated C–H bond and lowers the activation energy for C–H bond cleavage[89]. A calculation conducted by Weaver et al. predicted that the energy barrier for breaking the Pd-coordinated C–H bonds is lower by more than 100 kJ·mol^{-1} than those uncoordinated[90]. After the cleavage of C–H bond, the H or CH_3 spillovers to metal oxide surface to react with chemisorbed oxygen anions and CH_4 is then completely oxidized[91]. Compared with pure metal oxides which require high working temperature to activate C–H bond, the utilization of Pd lowers C–H bond cleavage energy barrier with consequent lower optimal temperature. The high CH_4 oxidation rate means the high electron injection rate and more chemisorbed oxygen participated in CH_4 oxidation, thereby enhancing the response of MOS CH_4 sensors.

Radical sensitization is considered as another possible effective approach. Various radicals (·OH, ·OR, $\cdot O_2^-$, etc.) could easily abstract a hydrogen atom from methane in a fast and exothermic reaction, realizing the activation of CH_4[93]. Therefore, the generation of abundant radicals on the surface of MOS could lead to the enhanced sensitivity, which could be combined with the above-mentioned light-illumination. This method has not yet been widely applied in CH_4 sensing, but already conducted in gas sensing. Wang et al. prepared Fe-doped hexagonal and monoclinic WO_3 phase junction materials to find their response to 10 ppm acetone to be 12 at 260 °C under light-emitting diode (LED) illumination, 3 times more than pristine WO_3. The proposed mechanism is that the formation of WO_3 phase junctions benefited the carrier separation, and Fe doping favored oxygen adsorption, which synergistically promoted the generation of superoxide radicals[94].

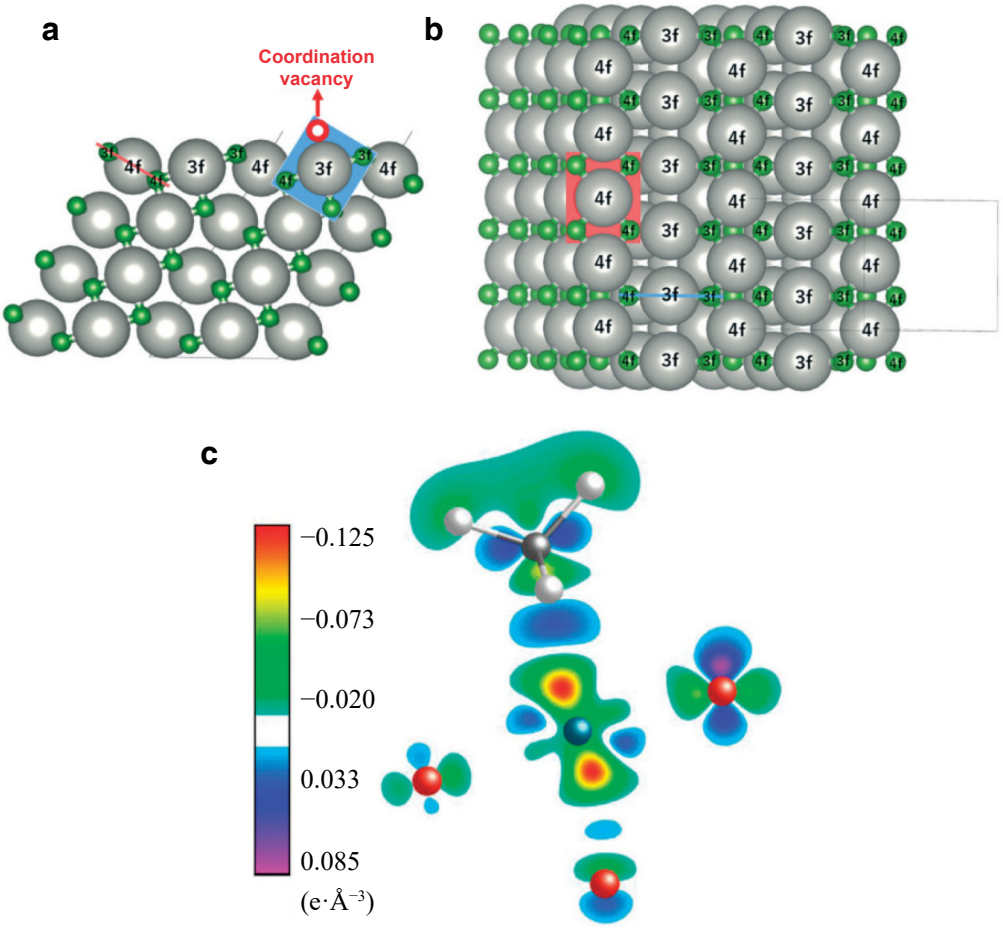

Fig. 7. The adsorption analysis of CH_4 on the PdO (101) surface. a, **b**, The side (a) and top (b) views of the slab model of the PdO (101) surface. Reproduced with permission from Ref.[92], © The Royal Society of Chemistry 2019. **c**, Different charge density plot by DFT for the σ-complex by adsorption of CH_4 on a cu-Pd site of PdO (101). Reproduced with permission from Ref.[89], © American Institute of Physics 2010.

The strategy of utilizing the water in the environment to further enhance the generation of free radicals has also been reported[95]. We have developed a photoactive room-temperature gas sensor based on MoS_2/Pt. Under light-irradiation, at room temperature and the humidity of 60%, the MoS_2/Pt sensor shows a significantly improved response (87.4%) to 100 ppm CO, greater than that in the humid, dark environment (< 10%) and that in the dry, light-illuminated environment (51.8%). It is confirmed that the MoS_2/Pt surface lowers the activation energy to convert CO to CO_2 via the free radicals ($\cdot O_2^-$ and ·OH) induced by the synergy of photochemical effects and water vapor[96].

2.2 Selectivity

Selectivity is an important parameter that determines the practicability of a sensor. A good selectivity means the specific response to the target analyte with slight or no response to the interfering gas. However, the weak selectivity is an intrinsic problem of MOS gas sensors, because any oxidative/reductive gas can induce the electron transferring on the surface of MOS[19]. More particularly, MOS sensors usually generate a weaker signal to CH_4 compared with other active molecules like CO, NO_2, NH_3, and ethanol due to its low reactivity. There are few literatures investigating the selectivity of MOS CH_4 sensors for now, and in some MOS CH_4 sensor researches the selectivity is not mentioned. In some cases that claim a good selectivity to CH_4, the response for interfering gas usually exceeds 10% of that for CH_4[97–100], which is high enough to cause a detection deviation in practice. In a case that uses porous three-dimensional (3D) hierarchical SnO_2 nanomaterials as sensing materials, the ethanol response exceeds 50% of CH_4 at the same concentration, and the response of formaldehyde is nearly the same as that of CH_4[101]. Besides, the aforementioned strategies to improve the sensitivity such as electronic and chemical sensitization also face the challenge of selectivity, since sensitization of MOS surface also increases the sensitivity to other gases. Even Pd was found to promote the dissociation or oxidation of CO[102], NH_3[103], and H_2[104]. Another problem in recent research is the choice of interfering gases. As summarized in **Table 1**, there are great differences in the choices of interfering gases. Hydrogen, ethanol, acetone, ammonia, and carbon monoxide are most commonly chosen in selectivity tests. Of course, the choice of interfering gas for selectivity test should be based on the actual application scenario to evaluate the practicality of the sensor.

2.2.1 *Operation temperature control*

Typically, the response to a certain gas of MOS sensors is time dependent with an optimal temperature at which the response is maximized. The temperature dependence of the response of MOS sensors is determined by several factors:

(1) Chemisorption of oxygen.

(2) Adsorption of target gas (CH_4, CO, NO_2, etc.) and their reaction with chemisorbed oxygen.

(3) Desorption of target gas and chemisorbed oxygen.

(4) The intrinsic charge carrier concentration.

At low temperature range, increasing temperature favors the first two processes more than the last two and the response to endow the increasing response. However, at high temperature, the desorption is accelerated with an increased intrinsic charge carrier, making the resistance change caused by gas reaction less significant, and the response is thereby reduced. Thus, competition among these processes determines the optimal temperature, and different gases have their own optimal temperature due to their distinct adsorption/desorption and reaction kinetics, as shown in **Fig. 8**[112].

Usually, CH_4 needs high temperature to trigger its oxidation on MOS surface compared to other reducing gas. For example, SnO_2 quantum dots showed a maximum response to CO at 225 °C, while at temperature above 375 °C the response to CH_4 is much higher[113]. Such dual selectivity can be further enhanced by supported catalyst since catalytic enhancement for different gas differs. Li et al. demonstrated an enhanced dual selectivity for detection of CO and CH_4 via PdPt nanoparticles-functionalized SnO_2 nanosheets. The PdPt/SnO_2 sensor showed a maximum response to CO and CH_4 at 100 and 320 °C, respectively. The enhanced dual selectivity was ascribed to the significant differences in the activation capacity of PdPt nanoparticles to CO and CH_4, since CO oxidation can be triggered by PdPt at 100 °C while CH_4 oxidation required a higher temperature[105]. However, one should admit that temperature control can only partially improve selectivity of MOS CH_4 sensors for the temperature profiles of the gas response are too broad and there might be gases which possess similar response-temperature distribution.

Table 1 Selectivity test in MOS CH_4 sensing

Materials	Operating temperature	Response to CH_4	Response to interfering gas	Response/recovery time	Ref.
PdPt/SnO_2	320 °C	5[a] (1000 ppm)	1.8[a] (CO), 2[a] (H_2S), 1.9[a] (NH_3), 50 ppm for all	5 s/4 s	[105]
Pd/SnO_2/rGO	Room temperature	5%[b] (4000 ppm)	0.5%[b] (CO), 0[b] (ethanol, NH_3, CO_2), 4000 ppm for all	5 min/7 min	[106]
Au/SnO_2	120 °C	8[a] (500 ppm)	1.95[a] (CH_3OH), 2[a] (ethanol), 3.2[a] (CH_2O), 2.9[a] ($CO(CH_3)_2$), 500 ppm for all	> 500 s/> 300 s	[107]
Au/VO_x	25 °C	25%[b] (1500 ppm)	0[b] (NH_3, ethanol, $CO(CH_3)_2$), 20%[b] (NO_2), 500 ppm for all	~ 1000 s/~ 1000 s	[108]
Pd/ZnO	200 °C	19.2[a] (5000 ppm)	4[a] (NH_3, 40 ppm), 2.3[a] ($C_6H_5CH_3$,1 ppm), 3[a] (CH_2O, 1 ppm), 2.4[a] (CH_3OH, 1 ppm)	~ 500 s/~ 300 s	[83]
SnO_2/rGO	150 °C	47.6%[b] (1000 ppm)	11.1%[b] (NH_3), 8.8%[b] (CO_2), 8.5%[b] (H_2O), 1000 ppm for all	61 s/330 s	[109]
Pt/Co_3O_4/MoS_2	170 °C	12.2%[b] (3000 ppm)	3%[b] (C_2H_6, CO), 2%[b] (H_2), 3000 ppm for all	~ 25 s/~ 20 s	[110]
Pt/SnO_2/MWCNTs	Room temperature	28.5%[b] (100 ppm)	15.5%[b] (NH_3), 4.6%[b] (CO_2), 100 ppm for both	176 s/763 s	[52]
Pd/SnO_2	300 °C	4.88[a] (250 ppm)	1.30[a] (CH_2O), 1.36[a] (C_6H_6), 1.23[a] ($C_6H_5CH_3$), 1 ppm for all	3 s/7 s	[111]

[a]The response is defined as R_a/R_g.
[b]The response is defined as $|R_a - R_g|/R_a$.

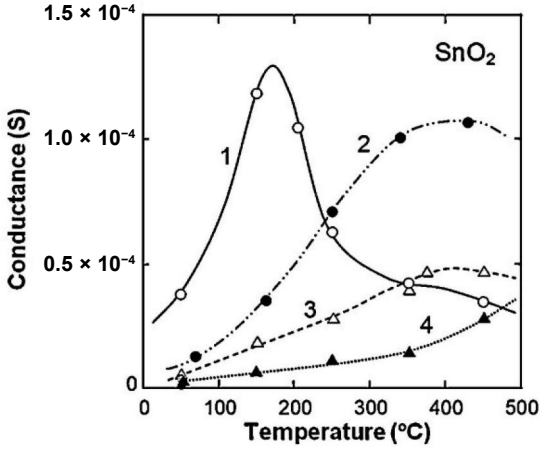

Fig. 8. Temperature dependence of conductivity response of SnO_2 thick films to (1) ethanol (50 ppm), (2) H_2 (500 ppm), (3) CO (300 ppm), and (4) CH_4 (1000 ppm) in dry synthetic air. Reproduced with permission from Ref.[112], © Elsevier B.V. 2004.

2.2.2 *Noble metal modification*

In the previous Section 2.1, it has been introduced that noble metal could act as chemical sensitizer to help improve the sensitivity of MOS-based CH_4 sensors due to their ability to catalyze methane oxidation. For the same principle, noble metal could also be utilized to improve the selectivity of CH_4, as long as its promotion effect to the catalytic oxidation of methane is stronger than that of other gases. Also as discussed before, noble metal such as Pd[83], Pt[110], Ag[114], and Au[107] as well as noble metal based bimetallic[105, 115, 116] structures could all help increase the selectivity, but Pd has the best effect for its capability to enhance C–H bond breakage. Wang et al. prepared In_2O_3 microspheres loaded with 6 wt.% Pd. At 50 °C, the response values of pristine In_2O_3 microspheres to 5000 ppm CH_4, 24 ppm CO, and 40 ppm NH_3 were 7.2, 2.8, and 2.5, respectively. Due to the heterojunction formed between Pd and In_2O_3 and the promoting effect of Pd on oxygen adsorption, the response values of the three gases increased to 22.7, 7.4, and 4.9, respectively. After the loading of Pd, the response ratio of CH_4 to CO and NH_3 increased from 2.57 and 2.88 to 3.07 and 4.63, respectively[117].

2.2.3 *Filter*

The additional filters incorporated into the sensor units or directly combined with sensing materials are one of the most effective ways to improve the selectivity. The interfering gas can be hindered by the size selection or physical adsorption, such as charcoal which is applied in CO sensors to adsorb butane, heptane, and ethanol[118], or dense SiO_2 layer that allows H_2 molecules to pass easily while the penetration of large molecules such as ethanol and CH_4 is hindered[119]. In addition to physical barrier filters, catalytically active filters can transfer some interfering gases into inactive species and thereby reduce the interference, which are more used than physical filters in CH_4 sensing. The stability of CH_4 can be utilized to improve CH_4 sensing selectivity since most interfering gases are more active than CH_4. Thus, these interfering gases can be pretreated via catalytic active filters. With a porous Ga_2O_3 catalyst-filter working at 800 °C, the response of interfering ethanol and acetone was reduced while the response to CH_4 slightly changed, as illustrated in **Fig. 9a**[120, 121]. The same ethanol catalytically filtration effect was also reported with an Al_2O_3 filtration layer on Pd/SnO_2 where the interference of ethanol was almost eliminated at above 400 °C while the sensitivity to CH_4 remains nearly unchanged. Filters such as Al_2O_3 and SiO_2 containing noble metals such as Pt and Pd were also reported to reduce the interference of ethanol in CH_4 sensing[122, 123]. Moreover, the interference cause by CO can also be reduced with a Pt-porous filter film deposited on the sensing film[124], because Pt has a low catalytic activity for the oxidation of CH_4 at temperature below 500 °C[125]. In a case sensing CH_4 via

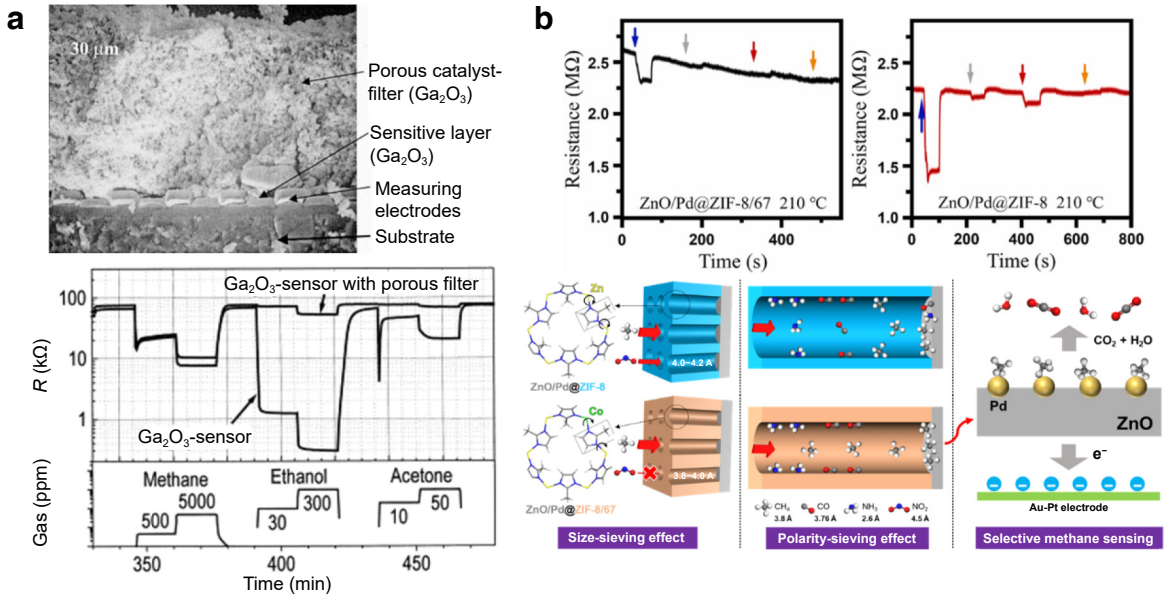

Fig. 9. Strategies for improving CH_4 selectivity via filter. a, Cross-section of the Ga_2O_3 catalytic filter and response curve of a pure Ga_2O_3 sensor and a sensor equipped with Ga_2O_3 catalyst filter to methane, ethanol, and acetone at 800 °C. Reproduced with permission from Ref.[121], © Elsevier Science S.A. 2000. **b**, Dynamic resistance curves of ZnO/Pd@ZIF-8/67 and ZnO/Pd@ZIF-8 to CH_4, CO, NH_3, and NO_2 at 210 °C, and schematic illustration of the dual sieving effect of ZIF-8/67 for selective CH_4 sensing against CO, NH_3, and NO_2. The blue, gray, red, and orange arrows represent CH_4, CO, NH_3, and NO_2 injection, respectively. Reproduced with permission from Ref.[133], © Elsevier Ltd. 2024.

Pt/SnO_2 with Au/Ce-Zr catalytic filter, the filter was found to reach nearly 100% conversion of CO, ethanol, toluene, acetone, and formaldehyde at 400 °C, while CH_4 conversion is relatively low (< 10%). Thus, the sensor showed highly selective response to CH_4[126].

Recently, the porous filters with a confined structure and definite pore diameters have been adopted in MOS-based gas sensing for the certainty and uniformity, which could well ensure the repeatability of filtering effect between sensors, and is helpful for designing the material to specifically improve the selectivity of a certain analyte against a certain interfering gas. Two types of the most representative applied filters are molecular sieves[127] and MOFs. Zhou et al. coated ZIF (a kind of MOF) onto ZnO nanorod arrays to form a core–shell structure, therefore ZIF could act as a filter to hinder the diffusion of gas with the dynamic diameter larger than the pore size of ZIF. The sensing performance turned out as predicted: The response of ZnO@ZIF to gases with smaller diameter approximately maintained the same as that of pristine ZnO nanorods, but suffered a significant decrease to gases with larger diameter[128]. From this point of view, CH_4 has the dynamic diameter of 3.8 Å[129], so filters with pore size bigger than 3.8 Å could be utilized to improve the selectivity of CH_4. For example, ZIF-8 is a potential candidate for its effective aperture of 4.0–4.2 Å[129], so we fabricated core–shell ZnO/Pd@ZIF-8 nanorods, decreasing the response of NO_2 with the dynamic diameter of 4.5 Å from 65.5% to 4.3%[130]. Moreover, as the gas adsorption capacity and property of MOF could be modulated by altering metal nodes[131] or ligands[132], we further introduced Co nodes to replace the original Zn nodes of ZIF-8 to form ZnO/Pd@ZIF-8/67 composites, which exhibited a response of 12.2% to 500 ppm CH_4 at 210 °C but no response to 50 ppm CO, 50 ppm NH_3, and 5 ppm NO_2. The enhanced polarity of ZIF by Co replacement favored the adsorption of polar CO and NH_3, while having little effect on nonpolar CH_4, thereby showing excellent selectivity (Fig. 9b)[133].

It should be mentioned that while the introduction of filters can improve the selectivity, they also slow down the diffusion process of CH_4 and O_2, which may decrease the sensitivity as well as prolong the response time. Also, both the physical filter and catalytical filter have the possibility of invalidation. The physical filter may reach adsorption saturation at a high concentration of interfering gas, and may lose its filtering property to interfering gas when the cell was saturated[134]. For the catalytical filter, the catalyst deactivation caused by poisoning or other factors should also be considered.

2.3 Stability

Stability is one of the most important factors to determine whether a sensor can be put into practice. A stability within 30 days is commonly seen in literatures to demonstrate the stability of MOS CH_4 gas sensors[114, 135]. However, it is difficult to investigate the stability of a sensor under laboratory conditions, because real situation is too complex to simulate. For example, currently the most used flammable gas sensors are catalytic combustion sensors in coal mines, which generate signals from the resistance change caused by the heat of catalytic combustion[136]. The main problem of this type of sensors is the catalyst poisoning and coking caused by other environmental gas in coal mine, which led to unstable signals and short device life[17].

Factors that influence the stability of MOS gas sensor have already been discussed in detail in a previous review[137]. Here some important factors especially for CH_4 sensing are discussed. (I) High temperature. A high temperature is usually required (usually ≥ 250 °C) owing to low reactivity of CH_4, together with a nanoscale grain size to increase its response[138–141]. However, high temperature leads to easier structure transformation for metal oxide. The mass transfer from smaller grains to larger grains leads to grain coarsening[142]. The structure transforming leads to the change in electrical property, thus resulting in the baseline drift with an unstable response for long-term devices[143]. (II) Catalyst deactivation. Generally, nanosized noble metal nanoparticles are often loaded on metal oxide for CH_4 catalytical oxidation to trigger electron transfer for CH_4 to MOS. Despite the aggregation of nanoparticle at high temperature, deactivations can result from other factors such as poisoning. For example, the exposure of Pd to SO_x or H_2S led to the formation of palladium sulfate and hinders CH_4 catalytic oxidation[144].

Some engineering approaches to improve stability and reliability of conductometric gas sensors have been reviewed[137], such as drift compensation, which use additional processing algorithms to compensate signal drift resulting from factors mentioned before[145]. Recently, machine learning-assisted[146] and neural network-assisted[147] signal calibration algorithms have also been adopted. However, despite these works on signal processing, it should be noted that engineering approaches could improve stability, but just within a limit. The main efforts should lay on the stability of sensitive material itself, which means the utilization of more thermal stable materials. However, the choice of stability and activity is always dilemma. On the one hand, to overcome the low reactivity of CH_4, the surface of metal oxides is modified with rich active sites to react with CH_4. On the other hand, the thermal stability of materials is reduced, causing a weak stability. For example, metal oxides with oxygen vacancies enriched surface are usually utilized to enhance sensing properties by increasing the number of adsorbed oxygen molecules[42, 148–150]. At an operation temperature of 200–500 °C, the diffusion of oxygen vacancies appeared despite its rather low diffusion coefficients[151, 152]. According to the oxygen-vacancy model, surface oxygen vacancies control the surface conductivity[153]. Thus, such diffusion can cause signal drifting of the devices in the long-term running. Another dilemma is the choice of grain size. As mentioned before, nanosized particles endow a high sensitivity with weak structure stability. In consideration of stability, the use of particles with extremely small size should be rejected, which means a reduced sensitivity[143]. The tradeoff between good stability and high sensitivity may have to be made in future research.

2.4 Humidity resistance

One of the biggest drawbacks in MOS gas sensors is their strong dependence on atmosphere humidity. Usually, researchers will set humidity at a value as a background like nitrogen or oxygen when conducting gas sensing tests. However, unlike nitrogen or oxygen with a relatively stable concentration, the humidity in atmosphere can vary at a wide range in practice due to many factors such as the weather or the ambient temperature. In fact, MOS itself can be applied as humidity sensor[154, 155]. The surface of most metal oxides is covered with hydroxyl groups due to atmosphere humidity. H_2O molecule splits to hydroxyl and neutral hydrogen atom[156]. Then hydroxyl bonds to Sn atom (SnO_2 as an example) while hydrogen atom bonds to the lattice oxygen to form "rooted" OH group. The built up rooted OH group has a lower electron affinity and serves as electron donor with an electron injection to conduction band.

Carbon Future

$$H_2O + Sn_{Sn} + O_O \leftrightarrow (Sn_{Sn}^{+} - OH^{-}) + (OH)_O^{+} + e^{-} \quad (4)$$

With increased humidity, the hydroxyl group would further adsorb H_2O molecules to form a physiosorbed layer and H_2O molecules layer, as shown in **Fig. 10**. In humidity sensing based on MOS, H^+ serves as charge carrier which hops between two adjacent hydroxyl groups at low humidity or hops between two H_2O molecules when continuous water layer is formed at high humidity[157, 158]. At this point, the influence of H_2O on MOS CH_4 sensing can be summarized as follows. Firstly, the adsorbed hydroxyl conduces to a decrease in baseline resistance of gas sensor due to electron injection, thus reducing the response to CH_4. Secondly, the adsorption of H_2O reduces active sites for oxygen chemisorption which is the key to CH_4 sensing. Besides, the hydroxyl or H_2O layer also inhibits CH_4 adsorption. Thirdly, with increased humidity, H^+ transferring is accelerated because the mobility of H^+ in continuous H_2O layer is higher than hopping between hydroxyls at low humidity, thus leading to a decreased response.

To the best of our knowledge, there are few reports on resistance to humidity in MOS CH_4 sensor. According to Licznerski et al., the as-prepared SnO_2/Pt showed a stable response to CH_4 in the humidity range of 7%–80% at an optimal temperature of 560 °C[159]. This is mainly because physisorption of H_2O become unstable at temperature above 100 °C, and surface hydroxyls start to desorb at temperature above 400 °C[160, 161]. It was reported that the chemisorption of OH group on the (110) facet was accompanied by the localization of negative charge on it to a greater extent than that in the case of OH group chemisorbed on the (101) facet of SnO_2[162]. This result provided a method that one can decrease humidity effects by controlling the morphology of crystal with proper facets exposed. Postica et al. found that Ag nanoparticles may act as hydroxyl absorbers since Ag-doped ZnO showed an improvement in stability under humidity changes than those undoped[163]. In addition to material modification methods, external approaches can also reduce the humidity influence. A facile way in practice is to build a H_2O filter to adsorb H_2O before it reaches sensing layer[164]. Another way is to integration of multiple sensors, for example, to fabricate temperature, humidity, and gas sensors on the same platform together[165, 166]. By means of signal processing, the signal drifting caused by humidity can be compensated to improve the accuracy of gas sensing. It should be noticed that some strategies can reduced the influence of external H_2O, while CH_4 oxidation can produce internal H_2O. The generated H_2O can desorb quickly at high temperature as mentioned before while at low temperature it can adsorb on the surface of metal oxides and hinder subsequent oxygen and CH_4 adsorption, thus reducing the sensing performances. Currently, there are few reports about the influence of the produced H_2O on low temperature MOS CH_4 sensing. Considering the hydroxylation of the surface and consequent physisorption of H_2O at low temperature, further investigation of low temperature MOS CH_4 sensing should take the produced H_2O into account.

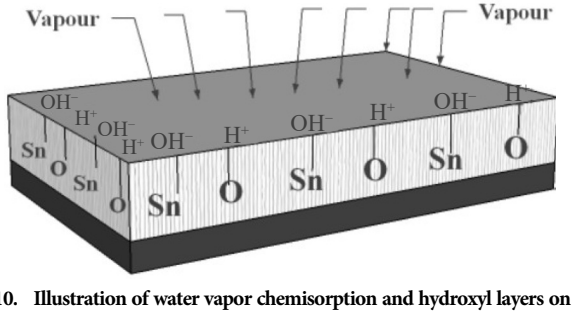

Fig. 10. Illustration of water vapor chemisorption and hydroxyl layers on the surface of SnO_2. Reproduced with permission from Ref.[156], © Farahani, H. et al. 2014.

3 Summary and perspective

At present, commercial CH_4 sensors are mainly infrared optical sensors and catalytic combustion sensors. The infrared optical CH_4 sensors are highly accurate with fast response (usually < 10 s) and a ppb-level detection limit[12]. However, the high cost in fabrication of the sensors limits their wide application. Though catalytic combustion CH_4 sensors have the advantage of low fabrication cost, high sensitivity to inflammable gas, and fast response (usually < 20 s), the risk of high operation temperature (~ 600 °C) and weak duration because of catalytic poisoning also hinder their further development. Compared with the two, MOS CH_4 sensors with a low fabrication cost, tunable structures, and satisfied stability are promising sensors in construction of intelligent CH_4 monitoring network or wearable devices in the future. Still, some key issues remain to be solved.

The fatal problem is the high working temperature required for CH_4 sensing. Typically, the temperature needed for MOS-based CH_4 sensing is above 150 °C, which increases the potential safety hazard considering the explosivity of CH_4. Most ideally, the hazard could be reduced to minimum if room-temperature CH_4 sensing could be achieved. In fact, the issue of decreasing the working temperature falls into the same category as the issue of improving the sensitivity, as higher sensitivity enables the sensor to work at a lower temperature while maintaining the same response to CH_4 of a certain concentration. However, current researches showed that at lower or room temperature, sensors will suffer from a long response/recovery time, often in minutes, which fails to meet the requirement of real-time CH_4 monitoring. Effective electronic sensitization and CH_4 activation at room temperature are the keys to fast, sensitive, and room temperature CH_4 sensing, and enhanced or novel strategies and methodologies might be proposed from this perspective.

Another problem is the weak selectivity of MOS CH_4 sensors. Though various methods have been applied to increase the response to CH_4, few of them are specific to CH_4 and the response to interfering gas is also enhanced. It seems that the interference caused by other gases can only be partially reduced and is impossible to be totally eliminated in MOS sensors if only by means of material modification. With the development of electronics and signal processing, an engineering approach is proposed to improve the selectivity of MOS sensors, namely sensor array. Based on the recognition that a single sensor cannot achieve selective sensing, sensor array is proposed, which means the integration of various sensors with different gas detection sensitivity[167, 168], as illustrated in **Fig. 11**. When the mixed gas is introduced and interacts with the sensor array, each sensor generates different signals, which means that the pattern of response across the sensors is distinct for different gases. By testing a large number of samples, a database is established for the sensor array. The unknown response pattern can be compared to the database and the unknown gas composition can be analyzed by means of signal processing. In a work of Kang et al., nanocolumnar films of metal oxides (pristine and Au-decorated

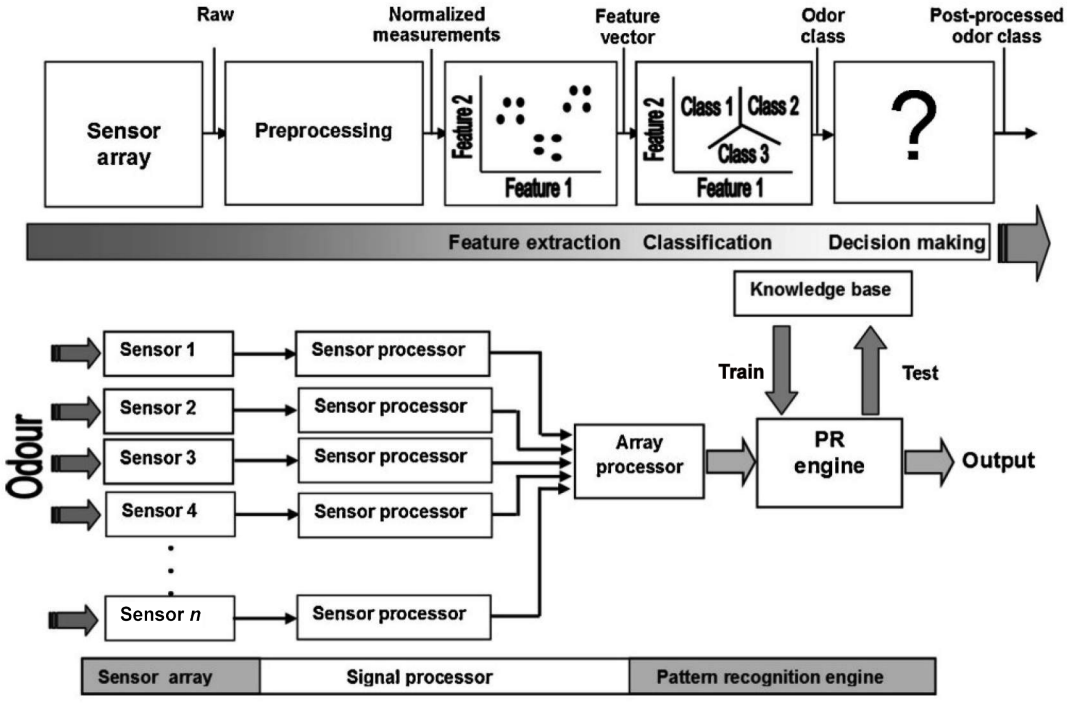

Fig. 11. Diagram illustrating the functioning of sensor array. Reproduced with permission from Ref.[170], © Elsevier B.V. 2013.

SnO_2, In_2O_3, WO_3, and CuO) were deposited with a high batch uniformity through glancing angle deposition. With this sensor array with 8 sensors and signal processing based on convolutional neural network, the real-time recognition of 6 gases (air, CO, NH_3, NO_2, CH_4, and C_3H_6O) was achieved with ~ 98% accuracy, and their concentrations could be estimated with the 10% error range in real time[169]. Nevertheless, it's worth noting that though sensor array provides a powerful solution to selectivity, the effort in improving single MOS CH_4 sensing is still significant since the accuracy of sensor array relies on the high sensitivity of each sensor.

The third problem lays on the fabrication process. First is the repeatability of MOS sensors. The sensing parameters depend on the microstructure of sensing materials, such as the grains connecting patterns. Present preparation methods of MOS consist of spin-coating[171], drop coating[172], magnetron sputtering[173], and screen printing[174], which are all based on the connection of powder samples to form conduction channels. In recent years, microelectromechanical system (MEMS) sensors consisted of both mechanical and electrical structures have been put out and widely applied in practical scenarios[175], and their repeatable and precise manufacturing process could help improve the repeatability and consistency of each sensor fabricated[176]. Though the problem of repeatability is barely mentioned in literatures, the distinct grain connecting patterns in each preparation lead to various sensing parameters of MOS sensors in different batches, which is not favored in practical production. Secondly, the additional cost might be introduced by new strategies. A typical example is the utilization of light-assisted MOS sensors, which require the additional optical units in device fabrication. Since the low cost is one of the advantages of MOS sensors over other types of sensors, a trade-off should be made between sensor improvements by introducing new strategies and the additional costs.

And the fourth problem is the humidity and stability. It is generally recognized that the existence of water will lead to the decrease of response of sensors, which may lead to a lower estimation of concentration under highly humid circumstances and cause safety hazards. From the aspect of sensitive materials, few general applicable strategies are proposed to improve the humidity resistance. According to the mechanism how humidity affects sensing, to modulate the adsorption of H_2O molecule on the surface of the material might be a possible approach, but the long-term stability of the modulation under working conditions is yet to be strenthened[177]. And if water is treated as another interference gas, then the tactics for improving sensitivity could also be suitable for improve humidity resistance. The method similar to sensor array might also work; another independent humidity sensor could be installed, and the response could be fabricated or analyzed concerning the current humidity[178]. The stability issue of MOS-based gas sensors is quite common, but more severe for CH_4 sensors due to the high working temperature and noble metal loaded for improving sensitivity. The contaminants in the environment are also an important factor to be concerned, as they might lead to the poisoning of the noble metal and the deterioration of the sensing performance. To our knowledge, the intrinsic low reactivity of CH_4 demands high activity of sensitive materials, which conversely contradicts the requirement of long-term stability. So, a proper balance should be established between high sensitivity and satisfying stability depending on the actual situations. Besides, the structural design and modulation, such as the introduction of single atom catalysts[116], and the effective filtering of contaminants might be able to further lengthen the life cycle of CH_4 sensors.

The increasing need for process safety and the development of CH_4 applications are pushing CH_4 sensing to become one of the most important parts of environmental monitoring. Present studies about CH_4 MOS sensing are still minor in the whole gas sensing field and far from practical. Further investigation of MOS CH_4 should still concentrate on the improvement of CH_4 sensitivity and

selectivity. The deeper understanding of the mechanisms of CH_4 sensing is also necessary, which helps to establish bottom-up fabrication of future sensors.

References

[1] Caballero, A.; Pérez, P. J. Methane as raw material in synthetic chemistry: The final frontier. *Chem. Soc. Rev.* **2013**, *42*, 8809–8820.

[2] Umeozor, E. C.; Jordaan, S. M.; Gates, I. D. On methane emissions from shale gas development. *Energy* **2018**, *152*, 594–600.

[3] Crow, D. J. G.; Balcombe, P.; Brandon, N.; Hawkes, A. D. Assessing the impact of future greenhouse gas emissions from natural gas production. *Sci. Total Environ.* **2019**, *668*, 1242–1258.

[4] Tu, Z. L.; Li, L.; Wang, F.; Zhang, Y. T. Review on separation of coalbed methane by hydrate method. *Fuel* **2024**, *358*, 130224.

[5] Demirbas, A.; Rehan, M.; Al-Sasi, B. O.; Nizami, A. S. Evaluation of natural gas hydrates as a future methane source. *Pet. Sci. Technol.* **2016**, *34*, 1204–1210.

[6] Liao, S. Y.; Cheng, Q.; Jiang, D. M. Gao, J. Experimental study of flammability limits of natural gas–air mixture. *J. Hazard. Mater.* **2005**, *119*, 81–84.

[7] Rodhe, H. A comparison of the contribution of various gases to the greenhouse-effect. *Science* **1990**, *248*, 1217–1219.

[8] Sher Shah, M. S. A.; Oh, C.; Park, H.; Hwang, Y. J.; Ma, M.; Park, J. H. Catalytic oxidation of methane to oxygenated products: Recent advancements and prospects for electrocatalytic and photocatalytic conversion at low temperatures. *Adv. Sci.* **2020**, *7*, 2001946.

[9] Wang, Y. L.; Hu, P.; Yang, J.; Zhu, Y. A.; Chen, D. C–H bond activation in light alkanes: A theoretical perspective. *Chem. Soc. Rev.* **2021**, *50*, 4299–4358.

[10] Anh, N. T.; Maurel, F. Use and misuse of frontier orbital theory. *New J. Chem.* **1997**, *21*, 861–871.

[11] Liu, F. M.; Zhang, Y. Q.; Yu, Y. S.; Xu, J.; Sun, J. B.; Lu, G. Y. Enhanced sensing performance of catalytic combustion methane sensor by using Pd nanorod/γ-Al_2O_3. *Sens. Actuators B: Chem.* **2011**, *160*, 1091–1097.

[12] Lin, S.; Chang, J.; Sun, J. C.; Xu, P. Improvement of the detection sensitivity for tunable diode laser absorption spectroscopy: A review. *Front. Phys.* **2022**, *10*, 853966.

[13] Sekhar, P. K.; Kysar, J.; Brosha, E. L.; Kreller, C. R. Development and testing of an electrochemical methane sensor. *Sens. Actuators B: Chem.* **2016**, *228*, 162–167.

[14] Mao, X. F.; Zheng, P. C.; Wang, X. F.; Yuan, S. Z. Breath methane detection based on all-optical photoacoustic spectrometer. *Sens. Actuators B: Chem.* **2017**, *239*, 1257–1260.

[15] Bassous, N. J.; Rodriguez, A. C.; Leal, C. I. L.; Jung, H. Y.; Lee, C. K.; Joo, S.; Kim, S.; Yun, C. H.; Hahm, M. G.; Ahn, M. H. et al. Significance of various sensing mechanisms for detecting local and atmospheric greenhouse gases: A review. *Adv. Sens. Res.* **2024**, *3*, 2300094.

[16] Chen, R. S.; Wang, J.; Xia, Y.; Xiang, L. Near infrared light enhanced room-temperature NO_2 gas sensing by hierarchical ZnO nanorods functionalized with PbS quantum dots. *Sens. Actuators B: Chem.* **2018**, *255*, 2538–2545.

[17] Bowen, W. Research on nonlinear calibration of mine catalytic-combustion-based combustible-gas sensor based on RBF neural network. *Heliyon* **2023**, *9*, e14055.

[18] Krishna, K. G.; Parne, S.; Pothukanuri, N.; Kathirvelu, V.; Gandi, S.; Joshi, D. Nanostructured metal oxide semiconductor-based gas sensors: A comprehensive review. *Sens. Actuators A: Phys.* **2022**, *341*, 113578.

[19] Korotcenkov, G.; Cho, B. K. Metal oxide composites in conductometric gas sensors: Achievements and challenges. *Sens. Actuators B: Chem.* **2017**, *244*, 182–210.

[20] Ji, H. C.; Zeng, W.; Li, Y. Q. Gas sensing mechanisms of metal oxide semiconductors: A focus review. *Nanoscale* **2019**, *11*, 22664–22684.

[21] Guo, Y. B.; Liu, C. C.; Wang, D. G.; He, R. Y. Advances in the development of methane sensors with gas-sensing materials. *Chin. Sci. Bull.* **2019**, *64*, 1456–1470.

[22] Dey, A. Semiconductor metal oxide gas sensors: A review. *Mater. Sci. Eng.: B* **2018**, *229*, 206–217.

[23] Jiao, M. Z.; Chen, X. Y.; Hu, K. X.; Qian, D. Y.; Zhao, X. H.; Ding, E. J. Recent developments of nanomaterials-based conductive type methane sensors. *Rare Met.* **2021**, *40*, 1515–1527.

[24] Kim, H. J.; Lee, J. H. Highly sensitive and selective gas sensors using p-type oxide semiconductors: Overview. *Sens. Actuators B: Chem.* **2014**, *192*, 607–627.

[25] Gautam, Y. K.; Sharma, K.; Tyagi, S.; Ambedkar, A. K.; Chaudhary, M.; Pal Singh, B. Nanostructured metal oxide semiconductor-based sensors for greenhouse gas detection: Progress and challenges. *R. Soc. Open Sci.* **2021**, *8*, 201324.

[26] Fu, L.; You, S. X.; Li, G. J.; Li, X. X.; Fan, Z. C. Application of semiconductor metal oxide in chemiresistive methane gas sensor: Recent developments and future perspectives. *Molecules* **2023**, *28*, 6710.

[27] Bai, S. L.; Liu, X.; Li, D. Q.; Chen, S.; Luo, R. X.; Chen, A. F. Synthesis of ZnO nanorods and its application in NO_2 sensors. *Sens. Actuators B: Chem.* **2011**, *153*, 110–116.

[28] China National Standard. 2019. Combustible gas detectors-Part 1: Point-type combustible gas detectors for industrial and commercial use [in Chinese] (GB 15322.1–2019).

[29] Vuong, N. M.; Kim, D.; Kim, H. Surface gas sensing kinetics of a WO_3 nanowire sensor: Part 2—Reducing gases. *Sens. Actuators B: Chem.* **2016**, *224*, 425–433.

[30] Brinzari, V.; Korotcenkov, G. Kinetic approach to receptor function in chemiresistive gas sensor modeling of tin dioxide. Steady state consideration. *Sens. Actuators B: Chem.* **2018**, *259*, 443–454.

[31] Zhang, S. S.; Li, Y. W.; Sun, G.; Zhang, B.; Wang, Y.; Cao, J. L.; Zhang, Z. Y. Synthesis of NiO-decorated ZnO porous nanosheets with improved CH_4 sensing performance. *Appl. Surf. Sci.* **2019**, *497*, 143811.

[32] Vuong, N. M.; Hieu, N. M.; Hieu, H. N.; Yi, H.; Kim, D.; Han, Y. S.; Kim, M. Ni_2O_3-decorated SnO_2 particulate films for methane gas sensors. *Sens. Actuators B: Chem.* **2014**, *192*, 327–333.

[33] Lu, W. B.; Ding, D. G.; Xue, Q. Z.; Du, Y. G.; Xiong, Y.; Zhang, J. Q.; Pan, X. L.; Xing, W. Great enhancement of CH_4 sensitivity of SnO_2 based nanofibers by heterogeneous sensitization and catalytic effect. *Sens. Actuators B: Chem.* **2018**, *254*, 393–401.

[34] Li, X.; Tan, T.; Ji, W.; Zhou, W. L.; Bao, Y. W.; Xia, X. H.; Zeng, Z. F.; Gao, Y. Remarkably enhanced methane sensing performance at room temperature via constructing a self-assembled mulberry-like ZnO/SnO_2 hierarchical structure. *Energy Environ. Mater.* **2024**, *7*, e12624.

[35] Zhang, Y. J.; Cao, J. L.; Wang, Y. Ultrahigh methane sensing properties based on Ni-doped hierarchical porous In_2O_3 microspheres at low temperature. *Vacuum* **2022**, *202*, 111149.

[36] Wang, Y.; Sun, X. Y.; Cao, J. L. Enhanced methane sensing performance of Ag modified In_2O_3 microspheres. *J. Alloys Compd.* **2022**, *895*, 162557.

[37] Chien, F. S. S.; Wang, C. R.; Chan, Y. L.; Lin, H. L.; Chen, M. H.; Wu, R. J. Fast-response ozone sensor with ZnO nanorods grown by chemical vapor deposition. *Sens. Actuators B: Chem.* **2010**, *144*, 120–125.

[38] Zhou, Q.; Chen, W. G.; Xu, L. N.; Peng, S. D. Hydrothermal synthesis of various hierarchical ZnO nanostructures and their methane sensing properties. *Sensors* **2013**, *13*, 6171–6182.

[39] Yang, X. Y.; Deng, Y.; Yang, H. T.; Liao, Y. Z.; Cheng, X. W.; Zou, Y. D.; Wu, L. M.; Deng, Y. H. Functionalization of mesoporous semiconductor metal oxides for gas sensing: Recent advances and emerging challenges. *Adv. Sci.* **2023**, *10*, e2204810.

[40] Zhu, X. J.; Zhang, X. L.; Chang, X. T.; Li, J. F.; Pan, L. K.; Jiang, Y. C.; Gao, W. X.; Gao, C. Y.; Sun, S. B. Metal-organic framework-derived porous SnO_2 nanosheets with grain sizes comparable to

Debye length for formaldehyde detection with high response and low detection limit. *Sens. Actuators B: Chem.* **2021**, *347*, 130599.

[41] Alenezi, M. R.; Alzanki, T. H.; Almeshal, A. M.; Alshammari, A. S.; Beliatis, M. J.; Henley, S. J.; Silva, S. R. P. A model for the impact of the nanostructure size on its gas sensing properties. *RSC Adv.* **2015**, *5*, 103195–103202.

[42] Al-Hashem, M.; Akbar, S.; Morris, P. Role of oxygen vacancies in nanostructured metal-oxide gas sensors: A review. *Sens. Actuators B: Chem.* **2019**, *301*, 126845.

[43] Luo, N.; Wang, C.; Zhang, D.; Guo, M. M.; Wang, X. H.; Cheng, Z. X.; Xu, J. Q. Ultralow detection limit MEMS hydrogen sensor based on SnO_2 with oxygen vacancies. *Sens. Actuators B: Chem.* **2022**, *354*, 130982.

[44] Hussain, T.; Kaewmaraya, T.; Khan, M.; Chakraborty, S.; Islam, M. S.; Amornkitbamrung, V.; Ahuja, R. Improved sensing characteristics of methane over ZnO nano sheets upon implanting defects and foreign atoms substitution. *Nanotechnology* **2017**, *28*, 415502.

[45] Yuan, H. Y.; Aljneibi, S. A. A. A.; Yuan, J. R.; Wang, Y. X.; Liu, H.; Fang, J.; Tang, C. H.; Yan, X. H.; Cai, H.; Gu, Y. D. et al. ZnO nanosheets abundant in oxygen vacancies derived from metal-organic frameworks for ppb-level gas sensing. *Adv. Mater.* **2019**, *31*, 1807161.

[46] Ahn, M. W.; Park, K. S.; Heo, J. H.; Park, J. G.; Kim, D. W.; Choi, K. J.; Lee, J. H.; Hong, S. H. Gas sensing properties of defect-controlled ZnO-nanowire gas sensor. *Appl. Phys. Lett.* **2008**, *93*, 263103.

[47] Tang, W.; Wang, J. Enhanced gas sensing mechanisms of metal oxide heterojunction gas sensors. *Acta Phys. Chim. Sin.* **2016**, *32*, 1087–1104.

[48] Miller, D. R.; Akbar, S. A.; Morris, P. A. Nanoscale metal oxide-based heterojunctions for gas sensing: A review. *Sens. Actuators B: Chem.* **2014**, *204*, 250–272.

[49] Zhang, S. S.; Li, Y. W.; Sun, G.; Zhang, B.; Wang, Y.; Cao, J. L.; Zhang, Z. Y. Enhanced methane sensing properties of porous NiO nanaosheets by decorating with SnO_2. *Sens. Actuators B: Chem.* **2019**, *288*, 373–382.

[50] Li, X. J.; Li, Y. W.; Sun, G.; Luo, N.; Zhang, B.; Zhang, Z. Y. Synthesis of a flower-like g-C_3N_4/ZnO hierarchical structure with improved CH_4 sensing properties. *Nanomaterials* **2019**, *9*, 724.

[51] Horastani, Z. K.; Sayedi, S. M.; Sheikhi, M. H. Effect of single wall carbon nanotube additive on electrical conductivity and methane sensitivity of SnO_2. *Sens. Actuators B: Chem.* **2014**, *202*, 461–468.

[52] Navazani, S.; Hassanisadi, M.; Eskandari, M. M.; Talaei, Z. Design and evaluation of SnO_2-Pt/MWCNTs hybrid system as room temperature-methane sensor. *Synth. Met.* **2020**, *260*, 116267.

[53] Kooti, M.; Keshtkar, S.; Askarieh, M.; Rashidi, A. Progress toward a novel methane gas sensor based on SnO_2 nanorods-nanoporous graphene hybrid. *Sens. Actuators B: Chem.* **2019**, *281*, 96–106.

[54] Lee, E.; VahidMohammadi, A.; Yoon, Y. S.; Beidaghi, M.; Kim, D. J. Two-dimensional vanadium carbide MXene for gas sensors with ultrahigh sensitivity toward nonpolar gases. *ACS Sens.* **2019**, *4*, 1603–1611.

[55] Wang, F. P.; Liu, H. C.; Hu, K. L.; Li, Y. Q.; Zeng, W.; Zeng, L. Hierarchical composites of MoS_2 nanoflower anchored on SnO_2 nanofiber for methane sensing. *Ceram. Int.* **2019**, *45*, 22981–22986.

[56] Mondal, B.; Das, J.; Roychaudhuri, C.; Mukharjee, N.; Saha, H. Enhanced sensing properties of ZnO-SnO_2 based composite type gas sensor. *Eur. Phys. J. Appl. Phys.* **2016**, *73*, 10301.

[57] Sahoo, T.; Kale, P. Work function-based metal-oxide-semiconductor hydrogen sensor and its functionality: A review. *Adv. Mater. Interfaces* **2021**, *8*, 2100649.

[58] Teichner, S. J. Recent studies in hydrogen and oxygen spillover and their impact on catalysis. *Appl. Catal.* **1990**, *62*, 1–10.

[59] Zhu, L. Y.; Ou, L. X.; Mao, L. W.; Wu, X. Y.; Liu, Y. P.; Lu, H. L. Advances in noble metal-decorated metal oxide nanomaterials for chemiresistive gas sensors: Overview. *Nano-Micro Lett.* **2023**, *15*, 89.

[60] He, Y. Y.; Jiao, M. Z. A mini-review on metal oxide semiconductor gas sensors for carbon monoxide detection at room temperature. *Chemosensors* **2024**, *12*, 55.

[61] Gai, L. Y.; Lai, R. P.; Dong, X. H.; Wu, X.; Luan, Q. T.; Wang, J.; Lin, H. F.; Ding, W. H.; Wu, G. L.; Xie, W. F. Recent advances in ethanol gas sensors based on metal oxide semiconductor heterojunctions. *Rare Met.* **2022**, *41*, 1818–1842.

[62] Kumar, R.; Liu, X. H.; Zhang, J.; Kumar, M. Room-temperature gas sensors under photoactivation: From metal oxides to 2D materials. *Nano-Micro Lett.* **2020**, *12*, 164.

[63] Li, Z. H.; Boda, M. A.; Pan, X. Y.; Yi, Z. G. Photocatalytic oxidation of small molecular hydrocarbons over ZnO nanostructures: The difference between methane and ethylene and the impact of polar and nonpolar facets. *ACS Sustain. Chem. Eng.* **2019**, *7*, 19042–19049.

[64] Liu, Z.; Xu, B. Y.; Jiang, Y. J.; Zhou, Y.; Sun, X. L.; Wang, Y. Y.; Zhu, W. L. Photocatalytic conversion of methane: Current state of the art, challenges, and future perspectives. *ACS Environ. Au* **2023**, *3*, 252–276.

[65] Melnick, D. A. Zinc oxide photoconduction, an oxygen adsorption process. *J. Chem. Phys.* **1957**, *26*, 1136–1146.

[66] Barry, T. I.; Stone, F. S. The reactions of oxygen at dark and irradiated zinc oxide surface. *Proc. R. Soc. Lond. A Math. Phys. Sci.* **1960**, *255*, 124–144.

[67] Wang, J.; Fan, S. Y.; Xia, Y.; Yang, C.; Komarneni, S. Room-temperature gas sensors based on ZnO nanorod/Au hybrids: Visible-light-modulated dual selectivity to NO_2 and NH_3. *J. Hazard. Mater.* **2020**, *381*, 120919.

[68] Zhai, J. L.; Wang, T.; Wang, C.; Liu, D. C. UV-light-assisted ethanol sensing characteristics of g-C_3N_4/ZnO composites at room temperature. *Appl. Surf. Sci.* **2018**, *441*, 317–323.

[69] Cui, J. B.; Shi, L. Q.; Xie, T. F.; Wang, D. J.; Lin, Y. H. UV-light illumination room temperature HCHO gas-sensing mechanism of ZnO with different nanostructures. *Sens. Actuators B: Chem.* **2016**, *227*, 220–226.

[70] Kimiagar, S.; Najafi, V.; Witkowski, B.; Pietruszka, R.; Godlewski, M. High performance and low temperature coal mine gas sensor activated by UV-irradiation. *Sci. Rep.* **2018**, *8*, 16298.

[71] Johnston, M. B.; Herz, L. M. Hybrid perovskites for photovoltaics: Charge-carrier recombination, diffusion, and radiative efficiencies. *Acc. Chem. Res.* **2016**, *49*, 146–154.

[72] Zhang, H. S.; Wang, Y.; Sun, X. Y.; Wang, Y. H.; Li, M. W.; Cao, J. L.; Qin, C. Enhanced CH_4 sensing performances of g-C_3N_4 modified ZnO nanospheres sensors under visible-light irradiation. *Mater. Res. Bull.* **2023**, *165*, 112290.

[73] Zhang, X. H.; Wang, C.; Zhang, M. L.; Luo, D. X.; Ye, S. Y.; Weng, B. Surface plasmon resonance-mediated photocatalytic H_2 generation. *ChemSusChem* **2024**, *17*, e202400513.

[74] Chen, X. X.; Li, Y. P.; Pan, X. Y.; Cortie, D.; Huang, X. T.; Yi, Z. G. Photocatalytic oxidation of methane over silver decorated zinc oxide nanocatalysts. *Nat. Commun.* **2016**, *7*, 12273.

[75] Reddy, N. L.; Rao, V. N.; Vijayakumar, M.; Santhosh, R.; Anandan, S.; Karthik, M.; Shankar, M. V.; Reddy, K. R.; Shetti, N. P.; Nadagouda, M. N. et al. A review on frontiers in plasmonic nano-photocatalysts for hydrogen production. *Int. J. Hydrogen Energy* **2019**, *44*, 10453–10472.

[76] Xia, Y.; Wang, J.; Xu, L.; Li, X.; Huang, S. J. A room-temperature methane sensor based on Pd-decorated ZnO/rGO hybrids enhanced by visible light photocatalysis. *Sens. Actuators B: Chem.* **2020**, *304*, 127334.

[77] Chen, R. S.; Wang, J.; Luo, S. R.; Xiang, L.; Li, W. W.; Xie, D. Unraveling photoexcited electron transfer pathway of oxygen vacancy-enriched ZnO/Pd hybrid toward visible light-enhanced methane detection at a relatively low temperature. *Appl. Catal. B: Environ.* **2020**, *264*, 118554.

[78] Li, X. Y.; Wang, C.; Tang, J. W. Methane transformation by photocatalysis. *Nat. Rev. Mater.* **2022**, *7*, 617–632.

[79] Burch, R.; Loader, P. K.; Urbano, F. J. Some aspects of hydrocarbon activation on platinum group metal combustion catalysts. *Catal. Today* **1996**, *27*, 243–248.

[80] Gensch, T.; James, M. J.; Dalton, T.; Glorius, F. Increasing catalyst efficiency in C–H activation catalysis. *Angew. Chem., Int. Ed.* **2018**, *57*, 2296–2306.

[81] Chen, Y.; Zhang, W. S.; Luo, N.; Wang, W.; Xu, J. Q. Defective ZnO nanoflowers decorated by ultra-fine Pd clusters for low-concentration CH_4 sensing: Controllable preparation and sensing mechanism analysis. *Coatings* **2022**, *12*, 677.

[82] Haridas, D.; Gupta, V. Enhanced response characteristics of SnO_2 thin film based sensors loaded with Pd clusters for methane detection. *Sens. Actuators B: Chem.* **2012**, *166–167*, 156–164.

[83] Wang, Y.; Meng, X. N.; Yao, M. X.; Sun, G.; Zhang, Z. Y. Enhanced CH_4 sensing properties of Pd modified ZnO nanosheets. *Ceram. Int.* **2019**, *45*, 13150–13157.

[84] Xue, D. P.; Wang, P. T.; Zhang, Z. Y.; Wang, Y. Enhanced methane sensing property of flower-like SnO_2 doped by Pt nanoparticles: A combined experimental and first-principle study. *Sens. Actuators B: Chem.* **2019**, *296*, 126710.

[85] Zhang, B.; Wang, Y.; Meng, X. N.; Zhang, Z. Y.; Mu, S. F. High response methane sensor based on Au-modified hierarchical porous nanosheets-assembled ZnO microspheres. *Mater. Chem. Phys.* **2020**, *250*, 123027.

[86] Li, M. W.; Sun, X. Y.; Wang, Y. H.; Qin, C.; Cao, J. L.; Wang, Y. Light-driven room temperature methane gas sensor based on Ag modified flower-like ZnO microsphere. *Sens. Diagn.* **2023**, *2*, 878–886.

[87] Hellman, A.; Resta, A.; Martin, N. M.; Gustafson, J.; Trinchero, A.; Carlsson, P. A.; Balmes, O.; Felici, R.; Van Rijn, R.; Frenken, J. W. M. et al. The active phase of palladium during methane oxidation. *J. Phys. Chem. Lett.* **2012**, *3*, 678–682.

[88] Mehar, V.; Kim, M.; Shipilin, M.; Van Den Bossche, M.; Gustafson, J.; Merte, L. R.; Hejral, U.; Grönbeck, H.; Lundgren, E.; Asthagiri, A. et al. Understanding the intrinsic surface reactivity of single-layer and multilayer PdO (101) on Pd (100). *ACS Catal.* **2018**, *8*, 8553–8567.

[89] Weaver, J. F.; Hakanoglu, C.; Hawkins, J. M.; Asthagiri, A. Molecular adsorption of small alkanes on a PdO (101) thin film: Evidence of σ-complex formation. *J. Chem. Phys.* **2010**, *132*, 024709.

[90] Weaver, J. F.; Hinojosa, J. A. Jr.; Hakanoglu, C.; Antony, A.; Hawkins, J. M.; Asthagiri, A. Precursor-mediated dissociation of n-butane on a PdO (101) thin film. *Catal. Today* **2011**, *160*, 213–227.

[91] Vottero, E.; Groppo, E.; Piovano, A. Supported metal nanoparticles-based catalysts and their interactions with H_2: Insights from inelastic neutron scattering spectroscopy. *ChemCatChem* **2024**, *16*, e202301127.

[92] Arevalo, R. L.; Aspera, S. M.; Nakanishi, H. Sulfation of a PdO (101) methane oxidation catalyst: Mechanism revealed by first principles calculations. *Catal. Sci. Technol.* **2019**, *9*, 232–240.

[93] Schwach, P.; Pan, X. L.; Bao, X. H. Direct conversion of methane to value-added chemicals over heterogeneous catalysts: Challenges and prospects. *Chem. Rev.* **2017**, *117*, 8497–8520.

[94] Wang, J. C.; Shi, W. N.; Sun, X. Q.; Wu, F. Y.; Li, Y.; Hou, Y. X. Enhanced photo-assisted acetone gas sensor and efficient photocatalytic degradation using Fe-doped hexagonal and monoclinic WO_3 phase-junction. *Nanomaterials* **2020**, *10*, 398.

[95] Li, X. X.; Wang, X.; Sun, Z. K.; Li, F. F.; Fu, Y.; Zhao, K. Y.; Zhao, G.; Zhu, C. G.; Xu, X. J. Surface free radicals activated CoP/MoS_2 sensors through electrocatalytic water splitting for enhanced NO_2 sensing at room temperatures. *Chem. Eng. J.* **2024**, *495*, 153381.

[96] Xia, Y.; Guo, S. H.; Yang, L.; He, S. F.; Zhou, L. X.; Wang, M. J.; Gao, J. Y.; Hou, M.; Wang, J.; Komarneni, S. Enhanced free-radical generation on MoS_2/Pt by light and water vapor co-activation for selective CO detection with high sensitivity. *Adv. Mater.* **2023**, *35*, 2303523.

[97] Han, L. Y.; Zhang, S. S.; Zhang, B.; Zhang, B. W.; Wang, Y.; Bala, H.; Zhang, Z. Y. Dual-selective detection of CO and CH_4 based on hierarchical porous In_2O_3 nanoflowers with Pd modification. *J. Materiomics* **2022**, *8*, 545–555.

[98] Bunpang, K.; Wisitsoraat, A.; Tuantranont, A.; Singkammo, S.; Phanichphant, S.; Liewhiran, C. Highly selective and sensitive CH_4 gas sensors based on flame-spray-made Cr-doped SnO_2 particulate films. *Sens. Actuators B: Chem.* **2019**, *291*, 177–191.

[99] Tshabalala, Z. P.; Shingange, K.; Dhonge, B. P.; Ntwaeaborwa, O. M.; Mhlongo, G. H.; Motaung, D. E. Fabrication of ultra-high sensitive and selective CH_4 room temperature gas sensing of TiO_2 nanorods: Detailed study on the annealing temperature. *Sens. Actuators B: Chem.* **2017**, *238*, 402–419.

[100] Anjitha, R. G.; Basu, P. K. Dual activation and photocatalyst-induced selective detection in defect tuned Pd-ZnO thin films for low ppm detection of CH and CO. *IEEE Sens. J.* **2023**, *23*, 143–153.

[101] Wang, Q.; Zhang, L. S.; Wu, J. F.; Wang, W. D.; Song, W. G.; Wang, W. A parallel solid-state NMR and sensor property study on flower-like nanostructured SnO_2. *J. Phys. Chem. C* **2010**, *114*, 22671–22676.

[102] Zhang, J. Y.; Shu, M.; Niu, Y. X.; Yi, L.; Yi, H. H.; Zhou, Y. S.; Zhao, S. Z.; Tang, X. L.; Gao, F. Y. Advances in CO catalytic oxidation on typical noble metal catalysts: Mechanism, performance and optimization. *Chem. Eng. J.* **2024**, *495*, 153523.

[103] Zhao, S. K.; Guan, B.; Zhuang, Z. Q.; Chen, J. Y.; Zhu, C. Y.; Hu, X. H.; Ma, Z. R.; Guo, J. F.; Dang, H. T.; Shu, K. Y. et al. Removing ammonia from exhaust gas through selective catalytic oxidation reaction: Research status and future perspectives. *J. Cleaner Prod.* **2024**, *467*, 142771.

[104] Shao, M. H. Palladium-based electrocatalysts for hydrogen oxidation and oxygen reduction reactions. *J. Power Sources* **2011**, *196*, 2433–2444.

[105] Li, G. J.; Wang, X. H.; Yan, L. M.; Wang, Y.; Zhang, Z. Y.; Xu, J. Q. PdPt bimetal-functionalized SnO_2 nanosheets: Controllable synthesis and its dual selectivity for detection of carbon monoxide and methane. *ACS Appl. Mater. Interfaces* **2019**, *11*, 26116–26126.

[106] Nasresfahani, S.; Sheikhi, M. H.; Tohidi, M.; Zarifkar, A. Methane gas sensing properties of Pd-doped SnO_2/reduced graphene oxide synthesized by a facile hydrothermal route. *Mater. Res. Bull.* **2017**, *89*, 161–169.

[107] Xue, D. P.; Zhang, Z. Y.; Wang, Y. Enhanced methane sensing performance of SnO_2 nanoflowers based sensors decorated with Au nanoparticles. *Mater. Chem. Phys.* **2019**, *237*, 121864.

[108] Liang, J. R.; Liu, J. F.; Li, N.; Li, W. J. Magnetron sputtered Au-decorated vanadium oxides composite thin films for methane-sensing properties at room temperature. *J. Alloys Compd.* **2016**, *671*, 283–290.

[109] Navazani, S.; Shokuhfar, A.; Hassanisadi, M.; Askarieh, M.; Di Carlo, A.; Agresti, A. Facile synthesis of a SnO_2@rGO nanohybrid and optimization of its methane-sensing parameters. *Talanta* **2018**, *181*, 422–430.

[110] Zhang, D. Z.; Chang, H. Y.; Sun, Y.; Jiang, C. X.; Yao, Y.; Zhang, Y. Fabrication of platinum-loaded cobalt oxide/molybdenum disulfide nanocomposite toward methane gas sensing at low temperature. *Sens. Actuators B: Chem.* **2017**, *252*, 624–632.

[111] Yang, L. P.; Wang, Z.; Zhou, X. Y.; Wu, X. F.; Han, N.; Chen, Y. F. Synthesis of Pd-loaded mesoporous SnO_2 hollow spheres for highly sensitive and stable methane gas sensors. *RSC Adv.* **2018**, *8*, 24268–24275.

[112] Tournier, G.; Pijolat, C. Selective filter for SnO-based gas sensor: Application to hydrogen trace detection. *Sens. Actuators B: Chem.* **2005**, *106*, 553–562.

[113] Mosadegh Sedghi, S.; Mortazavi, Y.; Khodadadi, A. Low temperature CO and CH_4 dual selective gas sensor using SnO_2

quantum dots prepared by sonochemical method. *Sens. Actuators B: Chem.* **2010**, *145*, 7–12.

[114] Wang, Y.; Cui, Y. Y.; Meng, X. N.; Zhang, Z. Y.; Cao, J. L. A gas sensor based on Ag-modified ZnO flower-like microspheres: Temperature-modulated dual selectivity to CO and CH_4. *Surf. Interfaces* **2021**, *24*, 101110.

[115] Zhang, W. S.; Yuan, T. W.; Wang, X. H.; Cheng, Z. X.; Xu, J. Q. Coal mine gases sensors with dual selectivity at variable temperatures based on a $W_{18}O_{49}$ ultra-fine nanowires/Pd@Au bimetallic nanoparticles composite. *Sens. Actuators B: Chem.* **2022**, *354*, 131004.

[116] Chu, T. S.; Rong, C.; Zhou, L.; Mao, X. Y.; Zhang, B. W.; Xuan, F. Z. Progress and perspectives of single-atom catalysts for gas sensing. *Adv. Mater.* **2023**, *35*, e2206783.

[117] Wang, Y.; Zhang, H. S.; Cao, J. L. Synthesis and low temperature methane sensing performance of Pd modified In_2O_3 microspheres. *Mater. Chem. Phys.* **2022**, *279*, 125749.

[118] Schweizer-Berberich, M.; Strathmann, S.; Göpel, W.; Sharma, R.; Peyre-Lavigne, A. Fillers for tin dioxide CO gas sensors to pass the UL2034 standard. *Sens. Actuators B: Chem.* **2000**, *66*, 34–36.

[119] Meng, X.; Zhang, Q. Y.; Zhang, S. P.; He, Z. The enhanced H_2 selectivity of SnO_2 gas sensors with the deposited SiO_2 filters on surface of the sensors. *Sensors* **2019**, *19*, 2478.

[120] Fleischer, M.; Meixner, H. Selectivity in high-temperature operated semiconductor gas-sensors. *Sens. Actuators B: Chem.* **1998**, *52*, 179–187.

[121] Fleischer, M.; Kornely, S.; Weh, T.; Frank, J.; Meixner, H. Selective gas detection with high-temperature operated metal oxides using catalytic filters. *Sens. Actuators B: Chem.* **2000**, *69*, 205–210.

[122] Wu, R. J.; Tian, L.; Li, H.; Liu, H. B.; Luo, J. X.; Tian, X. M.; Hua, Z. Q.; Wu, Y.; Fan, S. R. A selective methane gas sensor based on metal oxide semiconductor equipped with an on-chip microfilter. *Sens. Actuators B: Chem.* **2022**, *359*, 131557.

[123] Xu, J. Q.; Shun, Y.; Pan, Q. Y.; Qin, J. H. Sensing characteristics of double layer film of ZnO. *Sens. Actuators B: Chem.* **2000**, *66*, 161–163.

[124] Zhao, Y. X.; Wang, S. H.; Yuan, W. J.; Fan, S. R.; Hua, Z. Q.; Wu, Y.; Tian, X. M. Selective detection of methane by Pd-In_2O_3 sensors with a catalyst filter film. *Sens. Actuators B: Chem.* **2021**, *328*, 129030.

[125] Park, J.; Kim, D.; Byun, S. W.; Shin, H.; Ju, Y.; Min, H.; Kim, Y. J.; Heo, I.; Hazlett, M. J.; Kim, M. et al. Impact of Pd:Pt ratio of Pd/Pt bimetallic catalyst on CH_4 oxidation. *Appl. Catal. B: Environ.* **2022**, *316*, 121623.

[126] Fateminia, F. S.; Mortazavi, Y.; Khodadadi, A. A. Au-promoted Ce-Zr catalytic filter for Pt/SnO_2 sensor to selectively detect methane and ethanol in the presence of interfering indoor gases. *Mater. Sci. Semicond. Process.* **2019**, *90*, 182–189.

[127] Vilaseca, M.; Coronas, J.; Cirera, A.; Cornet, A.; Morante, J. R.; Santamaría, J. Use of zeolite films to improve the selectivity of reactive gas sensors. *Catal. Today* **2003**, *82*, 179–185.

[128] Zhou, T. T.; Sang, Y. T.; Wang, X. X.; Wu, C. Y.; Zeng, D. W.; Xie, C. S. Pore size dependent gas-sensing selectivity based on ZnO@ZIF nanorod arrays. *Sens. Actuators B: Chem.* **2018**, *258*, 1099–1106.

[129] Zhang, C.; Lively, R. P.; Zhang, K.; Johnson, J. R.; Karvan, O.; Koros, W. J. Unexpected molecular sieving properties of zeolitic imidazolate framework-8. *J. Phys. Chem. Lett.* **2012**, *3*, 2130–2134.

[130] Luo, S. R.; Chen, R. S.; Wang, J.; Xie, D.; Xiang, L. Designed synthesis of ZnO/Pd@ZIF-8 hybrid structure for highly sensitive and selective detection of methane in the presence of NO_2. *Sens. Actuators B: Chem.* **2021**, *344*, 130220.

[131] Shakya, D. M.; Ejegbavwo, O. A.; Rajeshkumar, T.; Senanayake, S. D.; Brandt, A. J.; Farzandh, S.; Acharya, N.; Ebrahim, A. M.; Frenkel, A. I.; Rui, N. et al. Selective catalytic chemistry at Rhodium(II) nodes in bimetallic metal-organic frameworks. *Angew. Chem., Int. Ed.* **2019**, *58*, 16533–16537.

[132] Wang, H.; Peng, J. J.; Li, J. Ligand functionalization in metal-organic frameworks for enhanced carbon dioxide adsorption. *Chem. Rec.* **2016**, *16*, 1298–1310.

[133] Chen, R. J.; Luo, S. R.; Xia, Y.; Xiang, L. Highly selective methane sensing based on enhanced dual sieving effects by ZnO/Pd@Co node-replaced ZIF-8 nanorods. *J. Environ. Chem. Eng.* **2024**, *12*, 112497.

[134] Krishna, R.; Van Baten, J. M. Describing mixture diffusion in microporous materials under conditions of pore saturation. *J. Phys. Chem. C* **2010**, *114*, 11557–11563.

[135] Zhang, S. S.; Li, J. T.; Han, L. Y.; Zhang, B. W.; Wang, Y.; Zhang, Z. Y. Preparation of porous NiO/In_2O_3 nanoflower-like composites and their dual selectivity for CO/CH_4. *Mater. Res. Bull.* **2023**, *165*, 112332.

[136] Wang, Y.; Tong, M. M.; Zhang, D.; Gao, Z. Improving the performance of catalytic combustion type methane gas sensors using nanostructure elements doped with rare earth cocatalysts. *Sensors* **2011**, *11*, 19–31.

[137] Korotcenkov, G.; Cho, B. K. Engineering approaches to improvement of conductometric gas sensor parameters. Part 2: Decrease of dissipated (consumable) power and improvement stability and reliability. *Sens. Actuators B: Chem.* **2014**, *198*, 316–341.

[138] Zhu, Y.; Hou, M.; Yang, L.; Zhang, S. P.; Zhang, G. Z.; Guo, S. H. A facile strategy to rapidly screening gas-sensitive materials in large samples: A case study of surface modified SnO_2 for CH_4 detection. *IEEE Sens. J.* **2024**, *24*, 15004–15010.

[139] Wang, X. H.; Li, Y. W.; Jin, X. H.; Sun, G.; Cao, J. L.; Wang, Y. Effectively improved CH_4 sensing performance of In_2O_3 porous hollow nanospheres by doping with Cd. *Langmuir* **2024**, *40*, 24740–24749.

[140] Jeon, I. S.; Bae, G.; Jang, M.; Yoon, Y.; Jang, S.; Song, W.; Myung, S.; Lim, J.; Lee, S. S.; Jung, H. K. et al. Atomic-level mediation in structural interparameter tradeoff of zinc oxide nanowires-based gas sensors: ZnO nanofilm/ZnO nanowire homojunction array. *Appl. Surf. Sci.* **2021**, *540*, 148350.

[141] Korotcenkov, G.; Han, S. D.; Cho, B. K.; Brinzari, V. Grain size effects in sensor response of nanostructured SnO_2- and In_2O_3-based conductometric thin film gas sensor. *Crit. Rev. Solid State Mater. Sci.* **2009**, *34*, 1–17.

[142] Lee, J.; Zhang, S.; Sun, S. H. High-temperature solution-phase syntheses of metal-oxide nanocrystals. *Chem. Mater.* **2013**, *25*, 1293–1304.

[143] Korotcenkov, G.; Cho, B. K. The role of grain size on the thermal instability of nanostructured metal oxides used in gas sensor applications and approaches for grain-size stabilization. *Prog. Cryst. Growth Charact. Mater.* **2012**, *58*, 167–208.

[144] Kim, K. J.; Lee, Y. L.; Hong, G. R.; Ahn, S. Y.; Kim, B. J.; Lee, S. S.; Jeon, Y.; Roh, H. S. A study on the activity recovery behavior of noble metal catalysts against sulfur poisoning. *Catal. Today* **2024**, *425*, 114361.

[145] Zhang, S. W.; Yuan, Z. Y.; Kong, L.; Wu, Z. X.; Meng, F. L. Drift-like effect compensation for the cyclic temperature operation of semiconductor gas sensor. *IEEE Trans. Ind. Electron.* **2025**, *72*, 2140–2149.

[146] Se, H.; Song, K.; Liu, H.; Zhang, W. Y.; Wang, X. H.; Liu, J. J. A dual drift compensation framework based on subspace learning and cross-domain adaptive extreme learning machine for gas sensors. *Knowl. Based Syst.* **2023**, *259*, 110024.

[147] Zhai, S. C.; Han, M. Y.; Li, Z.; Yang, S. J.; Duan, S. K.; Yan, J. M^2FL-CCC: Multibranch multilayer feature leaning and comprehensive classification criterion for gas sensor drift compensation. *IEEE Trans. Instrum. Meas.* **2023**, *72*, 2521312.

[148] Wang, J.; Hu, C. Y.; Xia, Y.; Zhang, B. Mesoporous ZnO nanosheets with rich surface oxygen vacancies for UV-activated methane gas sensing at room temperature. *Sens. Actuators B: Chem.* **2021**, *333*, 129547.

[149] Xu, H. Y.; Li, J. Z.; Fu, Y.; Tian, Y. W.; Yang, Z. D. Sensitized mechanism of recovered S-SnO_2 from tin sludge for CH_4 detection by increasing oxygen vacancy density as an efficient strategy. *Sens. Actuators B: Chem.* **2019**, *298*, 126838.

[150] Bonu, V.; Das, A.; Prasad, A. K.; Krishna, N. G.; Dhara, S.; Tyagi, A. K. Influence of in-plane and bridging oxygen vacancies of SnO_2 nanostructures on CH_4 sensing at low operating temperatures. *Appl. Phys. Lett.* **2014**, *105*, 243102.

[151] Carrasco, J.; Lopez, N.; Illas, F. First principles analysis of the stability and diffusion of oxygen vacancies in metal oxides. *Phys. Rev. Lett.* **2004**, *93*, 225502.

[152] Schaub, R.; Wahlström, E.; Rønnau, A.; Lægsgaard, E.; Stensgaard, I.; Besenbacher, F. Oxygen-mediated diffusion of oxygen vacancies on the TiO_2 (110) surface. *Science* **2003**, *299*, 377–379.

[153] Blackman, C. Do we need "ionosorbed" oxygen species? (Or, "a surface conductivity model of gas sensitivity in metal oxides based on variable surface oxygen vacancy concentration"). *ACS Sens.* **2021**, *6*, 3509–3516.

[154] Kumar, A.; Gupta, G.; Bapna, K.; Shivagan, D. D. Semiconductor-metal-oxide-based nano-composites for humidity sensing applications. *Mater. Res. Bull.* **2023**, *158*, 112053.

[155] Zhang, D. Z.; Wang, M. Y.; Tang, M. C.; Song, X. S.; Zhang, X. X.; Kang, Z. J.; Liu, X. H.; Zhang, J. H.; Xue, Q. Z. Recent progress of diversiform humidity sensors based on versatile nanomaterials and their prospective applications. *Nano Res.* **2023**, *16*, 11938–11958.

[156] Farahani, H.; Wagiran, R.; Hamidon, M. N. Humidity sensors principle, mechanism, and fabrication technologies: A comprehensive review. *Sensors* **2014**, *14*, 7881–7939.

[157] Agmon, N. The grotthuss mechanism. *Chem. Phys. Lett.* **1995**, *244*, 456–462.

[158] Jia, M.; Zhuang, Y. B.; Wang, F.; Zhang, C.; Cheng, J. Water-mediated proton hopping mechanisms at the SnO_2 (110)/H_2O interface from *ab initio* deep potential molecular dynamics. *Precis. Chem.* **2024**, *2*, 644–654.

[159] Licznerski, B. W.; Nitsch, K.; Teterycz, H.; Szecówka, P. M.; Wiśniewski, K. Humidity insensitive thick film methane sensor based on SnO_2/Pt. *Sens. Actuators B: Chem.* **1999**, *57*, 192–196.

[160] Egashira, M.; Kawasumi, S.; Kagawa, S.; Seiyama, T. Temperature programmed desorption study of water adsorbed on metal-oxides. I. Anatase and rutile. *Bull. Chem. Soc. Jpn.* **1978**, *51*, 3144–3149.

[161] Egashira, M.; Nakashima, M.; Kawasumi, S.; Selyama, T. Temperature programmed desorption study of water adsorbed on metal oxides. 2. Tin oxide surfaces. *J. Phys. Chem.* **1981**, *85*, 4125–4130.

[162] Wicker, S.; Guiltat, M.; Weimar, U.; Hémeryck, A.; Barsan, N. Ambient humidity influence on CO Detection with SnO_2 gas sensing materials. A combined DRIFTS/DFT investigation. *J. Phys. Chem. C* **2017**, *121*, 25064–25073.

[163] Postica, V.; Lupan, O.; Gapeeva, A.; Hansen, L.; Khaledialidusti, R.; Mishra, A. K.; Drewes, J.; Kersten, H.; Faupel, F.; Adelung, R. et al. Improved long‐term stability and reduced humidity effect in gas sensing: SiO_2 ultra‐thin layered ZnO columnar films. *Adv. Mater. Technol.* **2021**, *6*, 2001137.

[164] Kang, Y.; Ju, S. Graphene-filter-mounted tin-oxide-nanowire-transistor for chemical sensor. *Semicond. Sci. Technol.* **2018**, *33*, 125013.

[165] Wu, J.; Wu, Z. X.; Ding, H. J.; Wei, Y. M.; Yang, X.; Li, Z. Y.; Yang, B. R.; Liu, C.; Qiu, L.; Wang, X. T. Multifunctional and high-sensitive sensor capable of detecting humidity, temperature, and flow stimuli using an integrated microheater. *ACS Appl. Mater. Interfaces* **2019**, *11*, 43383–43392.

[166] Gugliandolo, G.; Naishadham, K.; Neri, G.; Fernicola, V. C.; Donato, N. A novel sensor-integrated aperture coupled microwave patch resonator for humidity detection. *IEEE Trans. Instrum. Meas.* **2021**, *70*, 9506611.

[167] Mei, H. X.; Peng, J. Y.; Wang, T.; Zhou, T. T.; Zhao, H. R.; Zhang, T.; Yang, Z. Overcoming the limits of cross-sensitivity: Pattern recognition methods for chemiresistive gas sensor array. *Nano-Micro Lett.* **2024**, *16*, 269.

[168] Verma, G.; Gokarna, A.; Kadiri, H.; Nomenyo, K.; Lerondel, G.; Gupta, A. Multiplexed gas sensor: Fabrication strategies, recent progress, and challenges. *ACS Sens.* **2023**, *8*, 3320–3337.

[169] Kang, M. G.; Cho, I.; Park, J.; Jeong, J.; Lee, K.; Lee, B.; Del Orbe henriquez, D.; Yoon, K.; Park, I. High accuracy real-time multi-gas identification by a batch-uniform gas sensor array and deep learning algorithm. *ACS Sens.* **2022**, *7*, 430–440.

[170] Korotcenkov, G.; Cho, B. K. Engineering approaches for the improvement of conductometric gas sensor parameters. *Sens. Actuators B: Chem.* **2013**, *188*, 709–728.

[171] Murugesan, M.; Meher, S. R. TiO_2-ZnO composite thin films fabricated by sol-gel spin coating for room temperature impedometric acetone sensing. *Sens. Actuators A: Phys.* **2024**, *369*, 115181.

[172] Pradeep, N.; Gopal, T. S.; Venkatraman, U.; Alrebdi, T. A.; Pandiaraj, S.; Alodhayb, A.; Muthuramamoorthy, M.; Kim, S. Y.; Le, Q. V.; Khan, S. H. et al. Effect of substrate bending towards chemiresistive based hydrogen gas sensor using ZnO-decorated MgO nanocubes. *Mater. Today Chem.* **2022**, *26*, 101200.

[173] Gao, W. X.; Chang, X. T.; Zhu, X. J.; Li, J. F.; Jiang, Y. C.; Wang, D. S.; Yang, C. X.; Sun, S. B. Al-doped ZnO/WO_3 heterostructure films prepared by magnetron sputtering for isopropanol sensors. *Rare Met.* **2024**, *43*, 247–256.

[174] R G, A.; Ahirwar, S.; Karthikeyan, L.; Subhash, J.; Singh, K.; Andhiwal, A.; Basu, P. K. Design, fabrication, and packaging of an optothermally activated nanocrystalline Pd-ZnO-based selective CO sensor on a screen-printed in-plane heater. *ACS Appl. Electron. Mater.* **2022**, *4*, 1651–1668.

[175] Hu, Q. M.; Dong, Z.; Zhang, G. X.; Li, Y. X.; Xing, S. F.; Ma, Z. H.; Dong, B. Y.; Lu, B.; Sun, S. H.; Xu, J. Q. Ultra-thin ALD CoO_x-ZnO heterogenous films as highly sensitive and environmentally friendly H_2S sensor. *Rare Met.* **2023**, *42*, 3054–3063.

[176] Asri, M. I. A.; Hasan, M. N.; Fuaad, M. R. A.; Yunos, Y. M.; Ali, M. S. M. MEMS gas sensors: A review. *IEEE Sens. J.* **2021**, *21*, 18381–18397.

[177] Tan, Y. L.; Li, S. C.; Yang, X.; Jin, B.; Sun, J. Strategies of improving anti-humidity performance for metal oxide semiconductors gas-sensitive materials. *Prog. Chem.* **2022**, *34*, 1784–1795.

[178] Naganaboina, V. R.; Bonam, S.; Anandkumar, M.; Suresh Deshpande, A.; Singh, S. G. Humidity-independent methane gas detection in $Gd_{0.2}La_{0.2}Ce_{0.2}Hf_{0.2}Zr_{0.2}O_2$-based sensor using polynomial regression analysis. *IEEE Electron Device Lett.* **2022**, *43*, 2153–2156.

Data availability

Not applicable.

Acknowledgements

This work was financially supported by the National Natural Science Foundation of China (Nos. 52274410 and 62101225), the Yunnan Fundamental Research Project (No. 202201AT070072), Project of the "Xingdian Talent Support Program" of Yunnan

Province (No. XDYC-QNRC-2022-0055), and the open project (KJS2306) of Jiangsu Key Laboratory for Carbon-Based Functional Materials & Devices, Soochow University.

Author contributions

R. J. C., S. Y. L. and Z. T. W. prepared the initial manuscript. Y. X. and L. X. revised the manuscript. L. X. supervised the study. All authors have approved the final version of the manuscript.

Competing Interests

The authors have no competing interests to declare that are relevant to this article.

Use of AI statement

None.